PINSTECH/NPD-122

KINEMATICAL ANALYSIS OF 2-, 3- AND 4- BODY CHANNELS IN THE REACTION (12.5 MeV/u) ^{84}KR + ^{nat}U OBSERVED WITH MICA TRACK DETECTORS

I.E. QURESHI, H.A KHAN, K. RASHID, P. VATER
R. BRANDT and P.A. GOTTSCHALK

NUCLEAR PHYSICS DIVISION
Pakistan Institute of Nuclear Science & Technology
P. O. Nilore Islamabad
September, 1987

PINSTECH/NPD-122

KINEMATICAL ANALYSIS OF 2-, 3- AND 4- BODY CHANNELS IN THE REACTION (12.5 MeV/u) $^{84}Kr + ^{nat}U$ OBSERVED WITH MICA TRACK DETECTORS

I.E. QURESHI, H.A. KHAN, K. RASHID, P. VATER[+]
R. BRANDT[+] and P.A. GOTTSCHALK[++]

Nuclear Physics Division
Pakistan Institute of Nuclear Science & Technology
P.O. Nilore, Islamabad, Pakistan

September 1987

[+] Kernchemie, FB-14, Philipps Universität, D-3550 Marburg, F.R. Germany
[++] Geselschaft für Reaktorsicherheit (GRS)mbH, D-5000 Köln, F.R. Germany

ABSTRACT

The exclusive measurements of reactions induced by 1050 MeV Kr ions incident on natural uranium have been made with the help of mica track detectors used in 2π-configuration. The cross-sections for ternary and quarternary events have been determined by directly counting the numbers of events of relevant multiplicities. The angular distribution in the case of elastic events has been fitted by generalized Fresnel model with parameters $\theta_{1/4} = 33.5^{\circ} \pm 0.5^{\circ}$ and $\Delta = 8.5 \pm 5$. A complete kinematical picture of the reaction process has been deduced by converting the three dimensional track parameters (lengths and angles) into parameters of reaction products (masses and energies) on an event by event basis. An empirical velocity-range relation has been used for this purpose, which has been obtained by an internal calibration procedure.

It has been found that the reaction mechanism for the bulk of the data can be described as a sequential fission process. However, non-equilibrium effects appear for a small number of events (8%) in the three-body channel and completely dominate the four-body channel. In the latter case a large mass trasfer ($\Delta m > 40u$) is found to occur during the first step of the reaction. Final mass distributions and total kinetic energy losses have been obtained for all channels. In order to estimate the uncertainties of computed quantities in relation to the measurement errors, Monte-Carlo simulation of the selected data sets has also been performed.

1. Introduction

General features of the heavy-ion reactions at energies below 10 MeV/u are now reasonably well-known [1-3]. In this energy region different reaction mechanisms are designated as quasi-elastic, deep-inelastic, quasi-fission (fast fission) and compound nucleus reactions with more or less well defined signatures for their identification. Experimentally it has become possible to differentiate the contribution of each reaction type at given entrance channel conditions by observing the reaction products with large area position senitive detectors operated in coincidence [4]. The classification of these reaction modes in terms of entrance angular momentum bins and the relation of these bins with qualitatively well-understood concepts of extra-push and extra-extra-push energies has recently been reported [5]. The influence of increasing bombarding energy on the reaction process is relatively less explored area. It is, therefore, important to carry out experiments at different intermediate energies to see how the low-energy mechanisms change and new phenomenon emerge. With an understanding that the boundaries between different reaction types are not sharp [6-8], it should still be possible to delineate the entrance channel conditions which favour the dynamical evolution of the strongly interacting system along a specific route. At energies above 10 MeV/u and with three or more fragments in the exit channel, an outstanding question is the manifestation of sequential fission process i.e. a process in which one

or both primary masses produced in the first step of the reaction subsequently undergo normal fission. The sequential nature of the process implies a complete decoupling of the two reaction steps as demonstrated in reactions of heavy nuclei at energies below 10 MeV/u studied with coincidence electronic counters [9,10]. At higher energies, the proximity and non-equilibrium effects have been found to be non-negligible [11,12], and at 15 MeV/u in ^{40}Ar induced reactions with different targets, the results could be explained by assuming the disintegration of a hot and fast rotating reaction composite into three fragments [13].

On the other hand Awes et al [14] have shown that the measured fission probabilities for the fragments resulting from $^{58}Ni+^{58}Ni$ reaction at 15.3 MeV/u are consistent with equilibrium fission calculations. Similar results have been reported for $^{100}Mo+^{100}Mo$ reaction in the energy region 12 - 19 MeV/u [15].

In the present paper we have done kinematical analysis of exclusive measurements for the reaction $^{84}Kr+^{238}U$ at 12.5 MeV/u in order to investigate the presence of sequential fission process. For this reaction, the entrance channel has no potential pocket ($Z_1.Z_2 > 3000$) and the composite system has no fission-barrier (fissility parameter > 1). Thus there is expected to be no compound nucleus formation and there would be vanishingly small quasi-fission component, if present at all. Furthermore, owing to the presence of a highly fissile reaction partner, there should be a preponderance of three fragments in the exit channel. The energy is, however, high enough to show some interesting departures from typical behavior observed at low energies above the Coulomb barrier. Of particular importance in the present study is the method of investigation. We have used a solid state nuclear track detector, SSNTD (mica in our case) to record the reaction products in an essentially exclusive manner. Whereas there are now an increasing number of experiments being performed with electronic counters in which complete kinematics can be determined, the earliest exclusive measurements were done with nuclear track detectors [16,17]. They are still useful as a complementary technique to electronic counters for low multiplicities and provide the only means of exclusive measurements for multiplicities greater than or equal to four. It is the object of this study to reemphasise the quantitative power of this technique.

The data pertaining to the tracks formed by the nuclear reaction products registered in an SSNTD were used to reconstruct the reaction kinematics numerically by Gottschalk et al [18], for the first time. They demonstrated the occurance of double-sequential fission in the reaction (1785 MeV) $^{238}U+^{nat.}U$ and (1535 MeV) $^{208}Pb+^{nat.}U$ on the basis of observed correlations in the relative velocities of final fragments. An estimate of the intrinsic spin distributions of primary fragments was also shown to be possible within their method. This technique was later explained in considerable detail in ref. [19]) and applied for the analysis of two-, three- and four-particle exit channels in the reaction (806 MeV) $^{84}Kr+^{nat.}U$. Detailed results for the reaction $^{238}U+^{nat.}U$ at 9.03 MeV/u obtained with glass [20]) and mica [21]) detectors and using the method of ref. 19 have been communicated since then. In all these reactions, it was shown that the sequential fission is the dominant mode of reaction mechanism. It was further shown by Khan et al [22]) that the angular distributuins of elastic events observed in mica detectors can be well represented by generalized Fresnel model [23]) as well as parameterized S-matrix method [24]).For the present reaction, we have determined the masses of final and intermediate reaction fragments, their kinetic energies and angular distributions alongwith the relative velocities of final fragments in order to understand the reaction mechanism. Measurements of total reaction cross-sections were made by direct counting of three-particle and four-particle events as well as through experimentally determined quarter-point angle. The angular distribution of elastic binary data has been fitted by generalized Fresnel model [23]). The reaction process which emerges through the kinematical analysis of this track data is on the whole consistent with the analysis of the same reaction at the lower energy of 9.6 MeV/u i.e. a deep-inelastic process in the first step of the reaction followed by equilibrium sequential fission of target-like fragments. There are, however, three importnant differences which can be attributed to higher radial injection energy which increases from 236 MeV to 452 MeV for s-waves in going from 9.6 MeV/u to 12.5 MeV/u.

I) The prefission mass distributions become broader

II) The mass drift in the first step of the reaction is increased

III) The non-equilibrium effects show up in the three-particle exit channel and completely dominate 4-particle exit channel.

The results pertaining to point (iii) have been reported elsewhere [25]), as well.

In the following, we describe the details of experimental set-up and data collection in sect. 2. The kinematical analysis of this data has been done with computer programme PRONGY [19]). In sect. 3, this method of analysis is described and it is shown how a complete kinematical picture of the reaction process is obtained by using correlated track data of each event of a given multiplicity. The information obtained from binary, ternary and quaternary events is discussed under seperate headings in sect. 4. Finally the main results are summed up in sect. 5.

2. Experiemental Set-up, Measurements and Data Selection

2.1) PRINCIPLE OF THE EXPERIMENTAL TECHNIQUE

The essential apparatus used in the present method is a thin slice of an insulator material coated with a fine layer of 'target'. This target-detector assembly is exposed perpendicularly to a bunched beam of heavy-ions having well-defined energies. The projectile ions enter the detector either without interaction with the target or cause any one of the possible nuclear reactions allowed under given enterance channel conditions. The ionization damage trails in the detector are formed by the projectiles in the former case and by the reaction products in the latter case. When the target layer is removed and the detector is treated in a suitable etchant, the particle tracks become visible under optical microscope, as thin hollow tubes. The 2π -geometry of this arrangement means that only those particles are registered which travel in the forward hemisphere. In terms of the multiplicity of the final reaction products, a number of processes can take place which are shown schematically in fig. 1 (a)-(f). In this figure, the tracks formed in the detector material are shown by hollow tubes and their projections on the plane of detector (which is also the plane of observation) are shown by solid lines. The physical information obtained through a given interaction process is indicated on top of the relevant figure. The track-lengths are not scaled, however, some typical lengths and angular

measurements noted in the present reaction are given in table 1 for the sake of orientation. Fig. 1(a) shows an uninteracted projectile which penetrates the detector normally and travels full length of its range in the detector. When viewed from the top, one can only see a black dot at the point of projectile enterance. The enumeration of these dots in selected areas is a direct measure of the fluence of the projectile beam. Fig. 1(b) shows a process in which there are definitely only two particles in the exit channel, since the projections of tracks on the detector surface are colinear. These events are termed as 'direct two-pronged events'. The lengths l_i and scattering angles $\xi_i^{(*)}$ of a selected set of these events representing elastic or quasi elastic reactions are used for the determination of quarter-point angle $\theta_{\frac{1}{4}}$ (see section 4.1). When the track projections are not colinear (Fig. 1c) then it is obvious that a third particle was present alongwith the two registered particles which could not be registered either because it had a mass lower than the detector threshold or it was emitted backwards in the laboratory system. These events are designated as 'indirect three-pronged events'. Fig. 1(d) is an example of 'direct three-pronged events' since the angle between any two track-length projections is less than 180°, indicating that the conservation of monentum is possible without requiring a missing mass. The categories of reactions indicated in fig. 1(c) and 1(d) are collectively used for the determination of the cross-section for three-particle exit channel, σ_3. A similar explanation can be given for the 'indirect four-pronged events' (fig. 1(e)) and 'direct four-pronged events' (fig. 1(f)) and so on for higher multiplicities. The kinematical analysis is carried out by using the measured lengths and angles of direct events of a given multiplicity. In practice, what is measured is the projected lengths of tracks, the depths of the track ends and the angles between projected lengths. The actual lengths and their angles with the projectile direction are calculated from these measurements.

2.2 EXPERIMENT

In the present experiment Muscovite mica of density 2.79 mg/cm^3 was used as track detector. Ten sheets of mica each having an area of

(*) The scattering angles in lab. frame as represented by symbol 'ξ' while in cm frame they are represented by 'θ'

12.57 cm^2 and a thickness of 100 μm were coated with the target material which was in the form of UF_4. The target thickness was measured to be in the range 0.9-1.6 mg/cm^2 for different detector plates. The exposures of these target-detector essemblies were done at UNILAC, GSI (Darmstadt, F.R. Germany) with a beam of 12.5 MeV/u, ^{84}Kr-ions incident perpendicular to the surface of the detector. The beam size was chosen to cover the entire detector area and to give a suitable dose of $2x10^6$ ions/cm^2. After exposures, the target was removed by treatment with HNO_3. The mica sheets were then etched for ten minutes at room temperature in 48% H_2F_2. This time is known to be sufficient for revealing full lengths of the tracks [26]. From the track-etching properties of mica, it has also been established [27] that only the particle of mass > 30u can be registered in it. Thus with the present experimental setup we made an exclusive recording of all reaction products with mass > 30u moving in the forward hemisphere.

2.3. SCANNING, MEASUREMENT AND SELECTION

The etched detectors were scanned by an optical microscope at a magnification of about 400x. By focussing the microscope on the surface, a large number of black dots could be seen corresponding to the points where incident particles entered the detector. The fluence with a maximum uncertainty of about 10% was found by enumerating these dots in randomly chosen areas. Based on previous experience [17-21], the heavy ion dose had been chosen such that the overlapping of these dots was extremely rare. In the next step, the direct and indirect events of different multiplicities (see sect. 2.1) were counted in selected areas for the calculation of cross-sections. The track lengths and angles of the direct events were measured by the following procedure. for each isolated interation of type shown in fig. 1(b), 1(d) and 1(f), the projected track lengths and angles between them (ϕ_{ij}) were measured with the help of a drawing tool (Leitz) attached to the microscope. The depths of the points where tracks end were measured with a linear displacement transducer (Heidenhain, METRO 1010) attached to the microscope stage holding the sample. Appropriate corrections were employed to take account of different refractive indices of air and the

detector material. The uncertainties in the measurements of projected lengths and depths were found to be $\pm$ 1.5 μm (standard deviation) and the uncertainties of angles between projected lengths was estimated to be $\pm$ 3° (standard deviation). It may be mentioned that the major source of these uncertainties is the not-so-well-defined end of track and the thickness as well as haziness of the projected-track view. The actual lengths l_i and polar angles ξ_i were calculated from these measurements and their uncertainties were determined by using standard quadratic error formulae. Also taken into account was the thickness of the target which had been sebsequently removed.

A 'data set' for an individual interaction of a given multiplicity, therefore, consists of four measurements for two-pronged events (l_1, l_2, ξ_1, ξ_2) nine measurements for three-pronged events (l_1, l_2, l_3, ξ_1, ξ_2, ξ_3, ϕ_{12}, ϕ_{23}, ϕ_{31}) and twelve measurements for four pronged events (l_1, l_2, l_3, l_4, ξ_1, ξ_2, ξ_3, ξ_4, ϕ_{12}, ϕ_{23}, ϕ_{34}, ϕ_{41}). Typical values of these quantities along with their uncertainties have been shown in table 1.

2.3.1 Two-pronged events

For two-pronged events 650 data sets were obtained which represented a subset of binary events involving elastic and quasi-elastic processes. (These two processes cannot be differentiated within the uncertainties of lengths and angular measurements). However 50 events were rejected because of large errors involved in their measurements (e.g. when the target recoils with such an angle that the etched track becomes very shallow). The remaining 600 events lie in a narrow region on the correlation plot between longest lengths and scattering angle (fig. 2). The frequencies for the track lengths and scattering angles of particles which are most probably projectile-like and target-like, are shown in fig. 3. Only a part of this group of data sets was used in the determination of quarter-point angle (see section 4.1). In view of a pre-selection of those events which did not diverge too much from the general trend of fig. 2, it was found difficult in later kinematical analysis (section 3.1) to estimate the contribution of deep-inelastic process towards the total reaction cross-section.

2.3.2. Three-pronged events

For three-pronged events a total of 815, direct and indirect events were observed. Only 167 of them were direct. However seven of these could not be measured. From the remaining direct events 40 were rejected because of large uncertainties involved in their measurements (shallow or very short tracks). Out of the 120 events used in kinematical analysis (see section 3.1), 6 events did not yield physical solutions, 7 events lied outside relative velocity window ($3.1 > v_{ij} > 1.7$). (This window for the relative velocities of the final fragments has been chosen on the basis of fission systematics. Also see section 4.2) and 27 events yielded total mass greater than 450 u. Thus only 80 events were finally selected for the detailed analysis discussed in section 4.2. The correlation plot for the longest track versus corresponding scattering angle for this channel is shown in fig. 4. In fig. 5 the frequency distributions for the track lengths and the corresponding angles are shown for the initial 160 data sets as well as the finally selected 80 data sets (hatched histogram).

2.3.3 Four-ponged events

There were only three direct four-pronged events in the entire detector areas apart from seven clearly discernable indirect four-pronged events. Two of the direct events could be analysed in detail as discussed in section 4.3. A summary of all events is given in table 2.

3. Method of analysis

3.1 DETERMINATION OF KINEMATICAL QUANTITIES FROM TRACK DATA

The correlated tracks formed by the heavy reaction products inside the detector material define three dimensional vectors which can be measured within the experimental uncertainties as discussed in section 2.3. The lengths of these vectors depend on the masses and velocities of

heavy-ion fragments as well as on the properties of the detector. In principle it is possible to determine the energy of a fragment of mass m and range R by inverting the range-energy relation,

$$R = m \int_{o}^{\beta} (dE/dx)^{-1} \beta \, d\beta \qquad (1)$$

where (dE/dx) is the stopping power which depends on the velocity ($v = \beta c$) and charge of the mass fragment apart from the parameters related with the properties of detector material. In practice, however, it is more convenient to use an empirical relation which expresses velocity 'v' as a function of track-length 'l' and mass 'm' of the registered particle. Following Gottschalk et al. [18], we use,

$$v = N_o \sum_{\mu=o}^{2} \sum_{\nu=o}^{4} c_{\mu\nu} m^{\mu} l^{\nu} \qquad (2)$$

where $c_{\mu\nu}$ are the detector-specific constants and N_o is an arbitrary scaling factor. The determination of these constants shall be discussed in section 3.2. The orders of polynomials for 'm' and 'l' in eq. 2. have been chosen on the basis of known behavior(e.g. Ref.28)of velocity-range curves i.e. whereas the velocity changes by an order of magnitude within the region of interest for the ranges (1.0 - 25.0 mg/cm^2), there is at most only 20% change in its value for the mass region A = 30 - 240, at a specific range. Thus a fourth order polynomial is required for length dependence but a second order polynomial is sufficient to represent mass dependence. Using this empirical relation, it is possible to determine the masses of rection products in 2-particle and 3-particle exit channel with the help of equations for momentum conservation i.e.

$$\sum_{i=1}^{N} m_i \vec{v}_i \, (l_i , m_i) = \vec{P}_{in} \qquad (3)$$

where $\vec{P}_{in}$ is the momentum of the projectile and 'N' is the multiplicity

of the event. The analytical solutions for the masses can be obtained from equations,

$$K_{2i}\, m_i^3 + K_{1i}\, m_i^2 + K_{0i}\, m_i = P_i \qquad (4)$$

where

$$K_{ni} = N_o \sum_{\nu=0}^{4} c_{n\nu}\, l_i^{\nu} \qquad (5)$$

The momentum P_i corresponding to the ith track can be written in terms of the observed track-parameters using simple geometrical considerations[29]). For the kinematical analysis of 4-particle exit channel, eqs. 2 and 3 are insufficient. In this case, one is in need to use an extra condition which may be the conservation of mass i.e

$$\sum_{i=1}^{N} m_i = m_P + m_T \qquad (6)$$

where m_P and m_T are the projectile and target masses respectively. With this condition, the closed-form solutions for the masses cannot be obtained, since eq. (3) now represents four non-linear coupled equations. The solutions may, however, be obtained by standard numerical methods[30]). For the sake of consistency, the 2-particle and 3-particle channel have also been analysed numerically in the present study, using the computer programm PRONGY[19]). The evaluation of masses is done iteratively by starting with a mass-independent velocity-range relation and substituting the first iteration masses in the mass-dependent velocity-range relation (eq.2) to be used in the second iteration. The final values of the masses are obtained if the ith iteration yields the same masses which were used in the rang-energy relation in the (i-1)th iteration. The computation of masses is done under the assumption of unperturbed kinematics. It is, however, obvious that the mass fragments which are responsible for the formation of observed tracks are only the 'secondary' masses. the 'primary' masses produced immediately after the collision are highly excited and they evaporate light particles which remain unregistered in the detector. However, it may be noted that the equations for the conservation of momentum are unchanged for the isotropic emission[31]) of light particles. Furthermore, it has been shown[19]) that the iterative algorithm used in the present study, determines the 'primary' masses and in facts slightly overestimates them.

This can be seen as follows. If m_p is the primary mass and m_s is the secondary mass, then the convergence of the iterative process is obtained for a computed mass 'm_c' which satisfies,

$$m_c \, v\,(1,m_c) = m_p v\,(1,m_s) \tag{7}$$

By Taylor's expansion of the two sides in terms of $\delta m = m_c - m_p$ and $\delta m' = m_p - m_s$, it can bee seen that

$$\delta m = -\,\delta m' \left(\varepsilon/1+\varepsilon\right) \tag{8}$$

The quantity $\varepsilon = m_p v^{-1}\, \partial_m v\,|_{m=m_p}$ is of the order of 10^{-1} for eq.2, so that δm is smaller than $\delta m'$ by an order of magnitude. It may be noted that $\delta m'$ is always positive and 'ε' is negative, so that δm is a positive quantity, which means that the computed masses are higher than primary masses. Thus, if the secondary mass is smaller than primary mass by say 10%, then the computed masses would be greater than primary masses by only 1%. Anyway, as mentioned previously, the dependence of range on the mass of the particle is not very strong. Therefore, within the accuracy of the experimental data, the computation of masses and velocities as described above is quite satisfactory.

3.2. CALIBRATION OF VELOCITY-RANGE RELATION

The coefficients appearing in eq.2 are highly sensitive with respect to the properties of the detector material. They may change even within different batches of the same material owing to slight variations of densities and compositions. It is, therefore, inevitable that these constants are determined in an internally consistent manner i.e the measured track data of the present reaction should be utilized to reproduce certain expected kinematical quantities. In the present study, the coefficients of eq.2 have been determined by the following procedure.

Starting with the set of coefficients obtained previously[17]), a number of velocity-range curves were obtained for different masses. By using three masses from the mass range 40-240 and five pairs of

velocity-range values for each of the chosen mass, it was established that the fifteen coefficients used initially can be reproduced. The velocity-range curves were then systematically modified and new sets of coefficients were obtained corresponding to each new modification. For any set of coefficients the output of kinematical quantities produced by the computer programm PRONGY was observed graphically. The modification of the velocity-range curve was continued until the following criteria were satisfied.

I. The track data of binary events, representing elastic and quasi-elastic processes should yield the distributions of two computed masses which should peak at the position of the projectile and target mass.

II. The TKEL computed by using binary track data should have a maximum near zero.

III. The distribution of total mass obtained by using track data of three-pronged event should be peaked at the value 322 u.
(The equation for mass conservation (eq.6) is redundant for 3-particle exit channel. Therefore it can be used as a calibration criterion).

In addition to the above criteria based on the track data of the reaction under study, it was checked whether the well-known mass and energy distribution of the fission-fragments of the reaction $^{235}U(n_{th},f)$ can also be reasonably well reproduced by the fitted coefficients. It may be noted that the requirement of meeting all these criteria simultaneously puts rather stringent constraints on the resulting velocity-range curves. This part of the present method is by far the most computer-time consuming. In the present analysis, the 600 data sets for binary elastic (& quasi-elastic) events were used and the resulting mass distributions were fitted by Gaussian distributions. The mean values of resulting mass distributions were found to be 84.2 u and 238.8 u with standard deviations of 6.5 u and 23.5 u respectively. The distribution of TKEL for these events was also fitted by a Gaussian of mean -2.3 MeV and standard deviation of 33.8 MeV. Fig. 6 shows a correlation plot of masses and TKEL alongwith the fitted Gaussian distributions for each quantity. For three-pronged events 80 data sets were used, which yield $m_{tot.}$ distribution with a mean of 322.9 u and

standard deviation 23.5 u. The fitted Gaussian distributions alongwith the experimental values of three-pronged as well as two-pronged events are shown in fig.7. The two-pronged track data pertaining to the fission fragments originating from the fission of ^{235}U induced by thermal neutrons was collected at two different laboratories (PINSTECH and Kernchemie Marburg University) by using mica track-detectors in 4π -configuration. In all, 207 data sets were measured and used for kinematical analysis. The mean values of the fission-fragments masses were computed to be 103 u and 135 u with a mean Q-value of 185 MeV. These procedures were employed to ensure that the determination of unknown masses and velocities is reliable and self-consistent. It is, however, more satisfactory to see if the resulting mass-dependent velocity-range curves are also consistent with other calculations based on different methods. For this purpose, we compared the results of Benton and Henke [32]) with present calculation. The calibrated velocity-range curves are shown by continous lines in fig.8. Also shown in this figure are the Benton and Henke values which agree with calibrated curves rather well. The deviations at the very high energy and for lighter masses have been repeatedly checked and found quite necessary for producing the correct mean value of projectile mass. (The region of velocity-range curve which is sensitive for this purpose is indicated fig.8). The deviations at low velocities lie in a region which is insensitive for the purpose of present calibration. The values of constants appearing in eq.2 are given in table 3.

3.3. MONTE CARLO SIMULATION FOR THE DETERMINATION OF UNCERTAINTIES IN COMPUTED QUANTITIES

As noted from the discussion of section 2, the experimental method of the present study is evidently not as accurate as electronic counters. Moreover it has been applied for the kinematical analysis of multifragment heavy-ion reactions only in a limited number of cases. As such, it is extremely necessary that the uncertainties of the computed quantities resulting from the uncertainties of measurements are determined for every investigated reaction, in order to establish mean uncertainties which could be considered accepted standards. In view of

this, we adopted a similar procedure for error analysis as used in previous communications based on the present method. A particular data set was chosen randomly from the data sets of a given multiplicity. Then, the measured lengths and angles of this chosen event were varied by using random numbers generated according to Gaussian distributions centered at the measured value and having standard deviations of 1/3 of the measured uncertainties. Thus a single data set was enlarged to 200 data sets having each of the measured quantity randomly distributed within experimental uncertainties. This enlarged group of data sets was then used in the computer program to obtain the distributions of kinematical quantities. Such distributions were further fitted by Gaussians whose standard deviations were regarded as experimental uncertainties of computed quantities. This procedure was repeated for a number of arbitrarily selected events for each multiplicity. Finally the mean values of the standard deviations obtained from the simulation of different events were regarded as the uncertainties of the relevant kinematical quantities. These values for two and three pronged events are shown in table 4. The four-pronged events are analysed purely by Monte-Carlo simulation and are discussed seperately in section 4.3.

4. Results and discussion

4. 1. CROSS-SECTIONS

With the present experimental technique, it is possible to determine the total reaction cross-section directly, by scanning the randomly selected areas of all the detectors and counting the number of events with multiplicity greater than or equal to three. An indirect method can also be employed which depends on the quarter-point angle i.e the angle at which the ratio of elastic differential cross-section to Rutherford differential cross-section falls to 1/4 as compared to its value at small angles (which is unity). The direct method relies on the knowledge of incident beam fluence (#/cm^2) and the target thickness (mg/cm^2). Both of these quantities can be determined with a maximum error of 10% in each case. This method, however, is beset with certain difficulties. In view of the presence of a large number of indirect events (see sect.

2.1) there is an appreciable group of events which can only be classified ambiguously. Thus, there is always the possibility that three- and four-pronged events remain 'hidden' in the larger group of binary events. Furthermore, the estimation of deep-inelastic binary events was found to be difficult in the present study. In a previous study of the same reaction at lower energy of 806 MeV[19]), this reaction precess was found to contribute more than 150 mb to the total cross-section. Table 5 shows the cross-section of individual channels of definite multiplicity and their resultant. The quoted uncertainties involve statistical errors as well as systematic errors.

The set of binary data representing elastic (and quasi-elastic) events can be used to obtain the angular distribution of the quantity $(d\sigma)_{exp.}/(d\sigma)_{Ruth.}$. In particular, we counted the number of events, summed over the azimuthal angle, lying in bins $(\theta_i-\theta_j)=2^{\circ}$ for the polar angle in order to calculate $2\pi\,(d\sigma/d\theta)_{exp.}$ which was divided by the corresponding theoretical value based on Rutherford scattering to evaluate the above mentioned ratio. The angular distribution of this ratio was fitted by the Fresnel model[23]) (Fig. 9). In the sharp cut-off approximation only a single parameter (i.e $\theta_{\frac{1}{4}}$) is used for fitting the experimental data. This fit has been shown by the broken line in fig. 9. The value of quarter-point angle was found to be $33.4^{\circ} \pm 0.5^{\circ}$ with $\chi^2 = 0.26$. As is evident this fit does not correctly reproduce the fall of the ratio $(d\sigma)_{exp}/(d\sigma)_{Ruth.}$ at angles greater than the region of quarter-point angle. It may be stressed that the experimental data for small angles has been intentionally omitted from the diagram since it falls very short of unity owing to the experimental bias. Moreover, this angular region is not relevant for the determination of quarter-point angle. The ascillations around unity at forward angles resulting from Fresnel diffraction model are also unreproducable within present experimental uncertainties. The fit at large angle can, however, be improved by using the generalized Fresnel model as shown by the continuous curve in fig. 9. The additional parameter 'Δ' (i.e. the angular momentum window) takes into account the smooth fall-off of the nuclear densities. The total reaction cross-section in this model is given by,

$$\sigma_R = \frac{\pi \Lambda^2}{k^2}\left[1 + \frac{2\Delta}{\Lambda} + \frac{\pi^2}{3}\frac{\Delta^2}{\Lambda^2}\right] \qquad (9)$$

where 'k' in the projectile wave-number and Λ is the variable associated with grazing angular momentum lg as $\Lambda = lg+1/2$. This is related to quarter-point angle by

$$\Lambda = \eta \cot (\tfrac{1}{2} \theta_{\frac{1}{4}}) \qquad (10)$$

where 'η' is the sommerfeld parameter

The calculated and fitted reaction parameters using elastic binary data are shown in table 6. The reaction cross-section obtained in this manner is shown under the heading of theoretical cross-section in table 5. The last column in this table is an estimate of the reaction cross-section which is independent from the present study. This has been obtained by using the expression for classical reaction cross-section

$$\sigma_R = \pi R_c^2 (1-V_c (R_c)/E_{c.m}) \qquad (11)$$

where R_c is the interaction radius, $V_c (R_c)$ is the coulomb barrier at this radius and $E_{c.m}$ is the energy in the centre-of-mass frame. For interacting nuclei with $(A_1^{1/3}+A_2^{1/3}) > 10$, the interaction radius has been fitted[33] by the expression

$$R_c/fm = 1.16 (A_1 + A_2)+2.4 \qquad (12)$$

This gives a value of R_c equal to 14.7 fm which is larger than that determined by using grazing angular momentum found in the present study i.e

$$R_{int} = [(\Lambda^2 + \eta^2)^{1/2} + \eta]/k = 13.7 \text{ fm} \qquad (13)$$

consequently this theoretical reaction cross-section is larger than either of the direct experimental or the theoretical cross-section based on experimental quarter-point angle. The latter two, however, reasonably agree with each other. If the strong absorption radii of ref.[34]) are used, the resulting total reaction would be 0.9% higher than that quoted in table 5. The discrepancy between the theoretical and experimental values of the total cross-section can be attributed to the missing deep-inelastic cross-section and unresolved quasi-elastic cross-section.

4.2. ANALYSIS OF THREE-PRONGED EVENTS

As described in section 2, there were 80 three pronged events whose track data was used in the detailed kinematical analysis. The three-particle exit channel is quite important from the point-of-view of understanding heavy-ion reaction mechanism. The kinematical quantities of interest for this purpose are the masses of the final reaction products, their velocity-vectors, scattering angles and total kinetic energy losses. all these quantities can be calculated for each event with the help of eqs. 2 and 3, within experimental uncertainties quoted in section 3.3. Owing to the presence of a highly fissile nucleus in the entrance channel, it is natural to look for the pairs of masses which can be correlated as fission fragments. The most convenient criterion for selecting such pairs in the present method is the absolute value of their realtive-velocity. It is known that the average value of this quantity can be described approximately by using fission energies systematics[34]) as

$$\langle |\vec{v}_i - \vec{v}_j| \rangle \simeq 0.2 \sqrt{(m_i+m_j)^{8/3}/m_i m_j} \qquad (14)$$

For the mass-splits of interest in this study[19]) the value of this quantity is expected to be (2.4±0.4)cm/ns.

For each of the 80 events, there was found to be at least one pair of mass whose relative velocity lies within one or two standard deviations of that range. However in 59 cases, another possible pair was also indicated when the criterion of relative-velocity alone was employed. This is due to the kinematical ambiguity as noted in the earlier analyses[19,20]). For each of these events the more appropriate pair is selected on the basis of a better agreement between the experimental and empirical fission Q-value. The distribution of relative velocities for all pairs selected in this manner is shown in fig. 10, where the arrow indicates the most probable velocity. On the basis of relative-velocity correlation, we can isolate the spectator mass from the pre-fission mass produced in the first reaction step. The distributions of the spectator and the pre-fission mass are shown in fig. 11. The mean values of the final fission fragment masses are also indicated on the same figure. It may be noted that one of the final masses m_j has a mean value equal to

the projectile mass. It would seem tempting, therefore, to regard this mass as the spectator and the other two masses as fission fragmnets of uranium. However, this would require that the reaction proceeds through either a quasi-elastic process or deep-inelastic process. In each case, one would expect the mean value of scattering angle to be in the vicinity of quarter-point angle. A distribution of the total events in different bins based on TKEL and mean scattering angle (fig. 12) shows that 40% of all events can be categorized as such. However 1/5 of the events in category II (see fig. 12) involve a mass transfer of more than 20 units while all events in category III involve about 30 units of mass. In category IV, the mass asymmetry has broad distribution centered not much below the initial asymmetry of 0.48. The consequence of these distributions is that the mean value of spectator mass is higher than the projectile mass. The above stated observations have been elaborated with the help of fig. 13 (a) and 13 (b), where the TKEL is plotted against mass asymmetry and the laboratory scattering angle. The arrows in these diagrams indicate the position of initial asymmetry (=0.48) and quarterpoint angle in laboratory frame (=24.9^{o}). It is of interest to note that in the TKEL region 150-450 MeV, there are two distinct group of events; one group involves scattering angles close to the quarter-point angle and in the other group the scattering angle is wider. the latter group also involves large mass transfer. By far, the largest group (32 events) involves TKEL $>$ 450, with a large distribution of masses exchanged between interacting nuclei.

On the basis of these observations, one can say that the three final masses observed in 80 investigated events of the present study arise due to a two-step process. (the two steps may not be completely decoupled[11]) In the first step, a quasi-elastic or a deep-inelastic or a quasi-fission process takes place, resulting in two excited masses and then in the second step, one of these masses fissions giving rise to two observed masses having relative-velocities within one or two standard deviations with respect to the mean value expected from fission systematics.

4.3. ANALYSIS OF FOUR-PRONGED EVENTS

The presence of four-pronged events in the reaction under study is a very interesting observation from the point of view of the underlying reaction mechanism. In an earlier communicaion[25]), we have interpreted this observation as an indication of quasi-fission process in the first step of the reaction followed by sequential fission (with or without mass equilibration) in the second step. As indicated in section 2.3, only three direct four-pronged events were observed in the total detector area of 125.7 cm^2. The projected lengths and the angles between them are shown in fig. 14. In one of these events (no.III in fig. 14), the projected length of one track was found to be very small (0.7μm) whereas the corresponding depth was comparatively very large (6.7μm). This indicated the path of a nuclear fragment making a very small angle (5.8^{o}) with the direction of the projectile motion. When this event was used in the kinematical analysis, unphysical masses ($m_i < 0$) were obtained. A number of variations in lengths and angles within experimental uncertainties were tried to see if physical masses can be obtained, however, the result was negative in all cases. Further it was checked whether this event was actually a three-pronged event with an artifact looking like a fourth prong. the total computed mass under this assumption turned out to be unacceptably large (i.e $>$ 570 u). Therefore it was concluded that this event could be a four-pronged event but experimetnal limitation render the track measurements extremely difficult. Thus it was included in the calculation of cross-secion but was rejected for kinematical analysis.

The remaining two events(no.I&II in fig. 14) were analysed by Monte-Carlo simulation. For this channel we produced 600 artificial events from each of the two data sets, following a procedure described in section 3.3. These enlarged groups of data sets were then treated like normal measured data sets in order to obtain the distributions of computed masses, scattering angles and velocities etc., of the reaction products. As in the case of three-pronged events, it is important to calculate the relative-velocities of reaction products in order to determine whether any pairs of masses can be regarded as fission fragments. thus we used the four final velocity vectors to compute six possible relative velocity combinations. These combinations constitute 3

complementary pairs of relative velocities i.e v_{ij} and v_{kl} ($i \neq j \neq k \neq l$ = 1,2,3,4). One such pair for event no. I and no. II is shown in fig. 15. The other combinations were found to lie outside three standard deviations from the mean of corresponding empirial value. It may be reminded that the gaussian distributions of computed quantities for this channel arise because of Monte-Carlo simulation of a single measurement. The standard deviations of these distributions, therefore, represent pure experimental uncertainties. The arrows on fig. 15 indicate the mean values of empirical relative velocities corresponding to the fission of equilibrated first step masses. The uncertainties in empirical values represent the uncertainties of computed masses. The final mass distribution for the two events are shown in fig. 16. In this figure, the pairs of masses whose relative velocities agree within three standard deviations with respect to the corresponding empirical values are marked and the relevant pre-fission mass is noted. The details of the computed kinematical variables are given in table 7. These results indicate the presence of a large mass transfer from the target to the projectile in the first step of the reaction yielding either two masses which both subsequently fission (one with and the other without mass equilibration) or the first reaction step yields three masses and one of these masses undergoes fission in the second step.

5. Conclusions

We have performed the kinematical analysis of $^{84}Kr+^{238}U$ reaction at 12.5 MeV/u on event to event basis by using the exclusive measurements of reaction products registered in muscovite mica. The total cross-section measured in this study falls short of the theoretical estimate based on nuclear radius systematics by about 10%. The angular distribution of elastic events (plus unresolvable quasi-elastic events) has been fitted by generalized Fresnel method and is found to be sensitive with respect to the angular momentum window parameter. Only a small subset of the total three-pronged events could be analysed numerically (table 2). The bulk of the analysed three-pronged data ($\sim$90%) is found to be consistent with the sequential fission process. The remaining events indicate the presence of non-equilibrium effects which were not observed at the lower energy of 9.6 MeV/u [19]. The conclusions of ref.[19] concerning the mass drift towards lesser asymmetry are confirmed, however this flow is found to be increased by about 20 u on the average. Also widths of the first step mass distributions are found to be enhanced from 24 u [19]) (E_{cm}=560 MeV) to 33 u (E_{cm}=776 MeV). For the TKEL window of 150 MeV - 450 MeV, the angular distribution of first step projectile-like mass is observed to lie in two seperate groups; one close to the quarter-point angle ($\theta_{1/4}$ =33.5°) and the other at more than double this angle. Higher TKEL (i.e> 450) involve a much wider angular distribution (σ_ξ =17) as well as higher width of final asymmetries (σ_η =0.2). The four-pronged events involve a large mass drift of 40 to 60 units in the first step accompanied by a kinetic energy loss which is 50-80% of the entrance centre-of-mass energy. The scattering angle is around 40° in the laboratory frame. These conditions strongly suggest that the first step of this reaction is a quasi-fission type process. The second step is found to be inconsistent with double-sequential fission process. The non-equilibrium fission is, however, indicated for only one of the first step masses while the other fragment seems to undergo normal fission. The experimental uncertainties of the kinematical parameters computed with the help of Monte-Carlo simulation (table 4) signify the quantitative power of this simple and inexpensive technique. It is, therefore, expected that this method would continue to play useful role

in the study of heavy ion reactions.

The authors wish to thank Dr. R. Spohr for kindly arranging the irradiations at the UNILAC (GSI, Darmstadt). The discussions with Dr. W. Westmeier and Dr. E.U. Khan and their assistance with the computational work is gratefully acknowledged. This work was carried out in the framework of the German-Pakistan agreement on scientific and technological cooperation. Thanks are due to International office, Kernforschungszentrum (kfK) and Pakistan Atomic Energy Commission for providing financial support to one of us (I.E.Q)

Table 1: Typical values of the three dimensional coordinates for tracks formed through reactions of different multiplicities, alongwith their uncertainties

Multiplicity of the event	l_1 (fm)	ξ_1 (degrees)	l_2 (fm)	ξ_2 (degrees)	l_3 (fm)	ξ_3 (degrees)	l_4 (fm)	ξ_4 (degrees)	ϕ_{12} (degrees)	ϕ_{23} (degrees)	ϕ_{34} (degrees)	ϕ_{41} (degrees)
2	88.4 ±1.5	18.3 ±1.0	5.0 ±1.5	79.3 ±17.2					180 ±3			
3	83.6 ±1.5	22.3 ±1.0	6.8 ±1.5	85.0 ±12.6	17.4 ±1.5	74.2 ±5.0			146.0 ±3	81.9 ±3	134.1 ±3	
4	18.6 ±1.5	47.7 ±4.6	18.0 ±1.5	19.9 ±4.8	27.9 ±1.5	61.5 ±3.1	21.9 ±1.5	57.1 ±3.9	115 ±3	09 ±3	143 ±3	93 ±3

Table 2: The number of multiprong events observed, scanned and analyzed for the reaction (1050 MeV) $^{84}Kr+^{238}U$

		Number of events		
		2-prong	3-prong	4-prong
Scanned	Direct		167	3
	Indirect		648	7
	Total		815	10
	Measured	650	160	3
	Analysed	650	120	3
	Selected	600	80	2

Table 3: Coefficients $c_{\mu\nu}$ of the empirical velocity-range relation (eq-2) in mica.

$N_o = 0.992$, Mica Density = 2.79 mg/cm^3

ν \ μ	0	1	2
0	9.599×10^{-2}	-1.057×10^{-3}	2.925×10^{-6}
1	2.5×10^{-2}	2.946×10^{-4}	-1.073×10^{-6}
2	9.613×10^{-6}	-2.795×10^{-5}	9.396×10^{-8}
3	-3.159×10^{-5}	8.743×10^{-7}	-2.435×10^{-9}
4	7.572×10^{-7}	-7.712×10^{-9}	1.081×10^{-11}

Table 4: The experimental uncertainties derived by Monte-Carlo simulation

Two-pronged events	Δm_P (u)	Δm_T (u)	Δ(TKEL) (MeV)
	3	16	30

Three-pronged events	Δm_k (u)	Δm_{ij} (u)	Δ(TKEL) (MeV)	Δv_{ij} (fm/10^{-23})
	3	18	20	0.006

Table 5: Cross-sections for the reaction 1050 MeV $^{84}Kr + ^{nat}U$

Experimental				Theoretical	
σ_3 (mb)	σ_4 (mb)	σ_5 (mb)	σ_{tot} (mb) $(= \sigma_3 + \sigma_4 + \sigma_5)$	$\sigma_R^{(a)}$ (mb)	$\sigma_R^{(b)}$ (mb)
3185±278	16±4	-	3201±282	3389±110	3929

(a)- Total reaction cross-section using experimentally determined quarter-point angle.

(b)- Classical total reaction cross-section assuming an interaction radius $R_c = 14.67$ (Wilczynski Ref. 33)

Table 6: Parameters of the reaction (1050 MeV) $^{84}Kr+^{nat}U$

Quantity	Value
Centre-of-mass energy	776.343 MeV
Projectile wave number-k	48.015 fm^{-1}
Sommerfeld parameter- η	147.53
Quarter-point angle- $\theta_{\frac{1}{4}}$ (c.m)	$(33.5+0.5)^{\circ}$
Angular momentum window- Δ	8.5+5
Coulomb barrier-V_c (R_C = 14.67 fm)	325.121 MeV
Grazing angular momentum- Λ	(490+?)$\hbar$
Interaction radius-R_{int}	(13.73+0.16)fm

Table 7: Kinematical quantities derived from the analysis of three dimensional track parameters in the case of two 4-pronged events observed in the reaction (1050 MeV) $^{84}Kr + ^{nat.}U$

	EVENT-I		EVENT-II	
First Step Masses (u)	(196+5)	(126+5)*	(143+7)	(179+7)*
First Step KInetic Energy Loss (MeV)	(408+20)		(654+10)	
Laboratory Scattering Angles (Degrees)	43.9	54.0*	44.8	24.5*
Final Masses (u)	(92+5)+(104+3)	(37+10),(89+6)	(59+8)+(84+4)	(76+4),((103+6)
Fission Q-values (MeV)	154.5	40.4*	96.1	139.5*
Relative Velocities (cm/ns)	(2.48+0.06)	(1.78+0.06)	(2.31+0.09)	(2.55+0.06)
Empirical Relative Velocities†(cm/ns)	(2.38+0.05)	(2.5+0.1)	(2.35+0.09)	(2.37+0.06)

*These quantities are valid if the second pair also results from a fission process in which the kinematics is distorted by final state interactions.

†according to Viola's systematics (Ref. 21)

References

1) R. Bass, Nuclear reactions with heavy ions (Springer Verlag, Berlin, 1980)

2) R. Bock, ed., Heavy ion collisions, Vol. II (North-Holland, Amsterdam, 1980)

3) D.A. Bromley , ed., Treatise on heavy-ion science, Vol. I-III (Plenum, New York, 1985)

4) J. Töke, R. Bock, G.X. Dai, A. Gobbi, S. Gralla, K.D. Hildenbrand, J. Kuzminski, W.F.J. Müller, A. Olmi, H. Stelzer, B.B.Back and S. Bjornholm, Nucl. Phys. A440 (1985) 327

5) A. van Geertruyden and Ch. Leclercq-Willain, Nucl. Phys. A459 (1986) 173

6) L. Adler, P. gonthier, J.H.K. Ho, A. Khodai, M.N. Namboodiri, J.B. Natowitz and S. Simon, Phys.Rev.Lett. 45 (1980) 696

7) J.M. Alexander, E. Duek and L. Kowalski, Z. Phys. A323 (1986) 83

8) Y. Blumenfeld, Ph. Chomaz, N. Frascaria, J.P. Garron, J.C. Tacmart, J.C. Roynette, D. Ardouin and W. Mittig, Nucl. Phys. A455 (1986) 357

9) D.v. Haarach, P. Glässel, Y. Civelekoglu, R. Männer and H.J. Specht, Phys.Rev.Lett. 26 (1979) 1728

10) T.C. Awes, R.L. Fergusson, R. Novotny, F.E. Obenshain, F. Plasil, V. Rauch, G.R. Young and H. Sann, Phys.Rev.Lett. 55 (1985) 1062

11) P. Glässel, D.v. Harrach, H.J. Specht and L. Grodzins, Z.Phys. A310 (1983) 189

12) D. Pelte, V. Winkler, J. Pochodzalla, M. Bühler, A. Gorks and B. Weissmann, Nucl. Phys. A438 (1985) 582

13) D. Pelte, U. Winkler, M. Bühler, B. Weissmann, A. Gobbi, K.D. Hildenbrand, H. Stelzer and R. Novotny, Phys.Rev. C34 (1986) 1673

14) T.C. Awes, R.L. Ferguson, R. Novotny, F.E. Obenshain, F. Plasil, V. Rauch, G.R. Young and H. Sann, Phys.Rev.Lett. 55 (1985) 1062

15) A. Olmi, P.R. Maurenzig, A.A. Stefanini, A. Gobbi and K.D. Hildenbrand, GSI Nachrichten 8-86 (Gesellschaft für Schwerionenforschung, Darmstadt)

16) R.L. Fleischer, P.B. Price, R.M. Walker and E.L. Hubbard, Phys.Rev. 143 (1966) 943

17) V.P. Perelygin, N.H. Shadieva, S.P. Tretyakova, A.H. Boos and R. Brandt, Nucl. Phys. A127 (1969) 577

18) P.A. Gottschalk, P. Vater, H.J. Becker, R. Brandt, R. Grawert, G. Fiedler, R.Haag and T. Rautenberg, Phys.Rev. Lett. 42 (1979) 359

19) P.A. Gottschalk, G. Grawert, P. Vater and R. Brandt, Phys.Rev. C27 (1983) 2703

20) R. Haag, G. Fiedler, R. Ulbrich, G. Breitbach and P.A. Gottschalk, Z. Phys. A316 (1984) 183

21) P. Vater, E.U. Khan, R. Beckmann, P.A. Gottschalk and R. Brandt, Nucl. Tracks, 11 (1986) 5

22) H.A. Khan, I.E. Qureshi, W. Westmeier, R. Brandt and P.A. Gottschalk Phys.Rev. C32 (1985) 1551

23) W.E. Frahn, Nucl. Phys. A302 (1978) 301

24) J.A. McIntyre, K.H. Wang and L.C. Becker, Phys.Rev. 117 (1960) 1337

25) I.E. Qureshi, H.A. Khan, K. Rashid, P.A. Gottschalk, P. Vater and R. Brandt, submitted to Phys. Rev.

26) H.A. Khan, G. Tress, P. Vater and R. Brandt, Nuclear Tracks 4 (1980) 109

27) H.A. Khan and S.A. Durrani, Nucl. Instrum. Meth. 98 (1972) 229

28) L.C. Nothcliffe and R.F. Schilling, Nucl.Data Tables A7 (1970) 233

29) H.A. Khan, I.E. Qureshi, K. Jamil, P.A. Gottschalk, P. Vater and R. Brandt,To Appear in Nucl. Instrum. Meth. (1986).

30) M.J.D. Powell in Numerical methods for non-linear algebraic equations, ed. P. Rabinowitz (Gordon & Breach, London, 1970)

31) B. Tamain, R. Chechik, H. Fuchs, F. Hanappe, M. Morjean, C. Ngo, J. Peter, M. Dakowski, B. Lucas, C. Mazur, M. Ribrag and C. Signarbieux Nucl. Phys. A330 (1979) 253

32) E.V. Benton and R.P. Henke, Nucl. Instrum. Meth. 67 (1969) 87

33) J. Wilczynski, Nucl. Phys. A216 (1973) 386

34) V.E. Viola Jr., Nucl. Data Sect. A1 (1966) 391

FIGURE CAPTIONS

Fig. 1: Schematic representation of multi-prong events observed with an SSNTD. The hollow tubes are the actual tracks formed by the reaction products. Thick lines are the projected lengths observed with the microscope. In practice, these lines are somewhat irregular in shape and hazy at the ends. Also measured with the microscope are the depths (broken lines) and angles between track-projections (ϕ_{ij}). Actual lengths (l_i) and polar angles (ξ_i) are deduced from these measurements. (a) an uninteracted projectile , (b) a direct binary event, (c) an indirect ternary event (d) a direct ternary event ((c) and (d) together determine the cross-section for three pronged events i.e σ_3), (e) an indirect quarternary event, (f) a direct quarternary event. ((e) & (f) together determine the cross-section for four-pronged events).

Fig. 2: Correlation plot for the longer length and the corresponding scattering angle in the case of $^{84}Kr+^{nat}U$, binary reactions observed at 12.5 MeV/u. Track lengths which deviate too much from the bulk of data represent inelastic events (not shown).

Fig. 3: Frequency distributions for the track lengths and scattering angles of projectile and target. These histograms show the 'selected' 600 events, representing the elastic (quasielastic) subset of binary data.

Fig. 4: Correlation plot for the longest length and the corresponding scattering angle in the case of $^{84}Kr+^{nat}U$, ternary reactions at 12.5 MeV/u. These events are consistent with the sequential fission process as shown in sect. 4.3.

Fig. 5: Frequency distributions for the track lengths and scattering angles of the longest track and the sum of the other tracks for the total set (160 events). Also shown by hatched histograms are the frequency distributions of the longest track and the corresponding scattering angle in the case of finally selected

80, ternary events.

Fig. 6: Correlation plot of the masses of two-body exit channel integrated over all angles and the TKEL for $^{84}Kr+^{nat}U$ at 12.5 MeV/u. The data corresponds to elastic (quasi-elastic) binary events and is uncorrected for the experimental uncertainties. The fitted gaussians for projectile-like masses (84.2 $\pm$ 6.5 u), target-like masses (238.8 $\pm$ 23.5 u) and TKEL (-2.3 $\pm$ 33.8 MeV) indicate the applicability of coefficients (table 3) used in the velocity-range relation, eq. 2.

Fig. 7: Distributions of computed total masses in the two- and three-body exit channels in $^{84}Kr+^{nat}U$ reaction at 12.5 MeV/u. The solid and dashed lines refer to Gaussian fits with σ_{2m} = 23 u, σ_{3m} = 47 u respectively. The data have not been corrected for experimental uncertainties.

Fig. 8: Empirical velocity-range curves corresponding to eq. 2 and table 3, obtained after completing internal calibration procedure. For comparison the calculations based on Benton and Henke's program (ref. 32) for the projectile, ^{84}Kr (triangles) and the target, ^{238}U (squares) incident on mica are also shown. The regions of ranges which are most sensitive for fitting projectile and target masses are indicated by horizontal bars.

Fig. 9: Ratios of the experimental differential cross-section to the Rutherford cross-section as a function of the scattering angle in c.m frame, for the reaction ^{84}Kr + ^{238}U at 12.5 MeV/u. The data corresponds to the subset of elastic and quasi-elastic events. The dashed line shows a one parameter fit based on Fresnel model and the full line represent two parameter fit based on generalized Fresnel model (Ref. 23)

Fig. 10: The distribution of the relative velocity of one pair of final masses in each of the 80 ternary events studied in the reaction ^{84}Kr + ^{238} at 12.5 MeV/u. The pair of meaasses whose relative velocity lies within the above histogram is recognised as

fission fragments. The arrow shows the value of most probable velocity, 2.48 cm/ns.

Fig. 11: The gaussian fits for the spectator and the pre-fission mass in the three-body channel of reaction $^{84}Kr + ^{238}U$ at 12.5 MeV/u. The computed final masses m_i, m_j are also shown on the diagram. The identification of fissioning fragment is based on the relative velocity correlation of fig. 10.

Fig. 12: The distribution of ternary events with respect to TKEL and scattering angle of projectile-like fragment. For each TKEL bin, an average value of scattering angle ($\overline{\xi}$) is indicated. Events in bin I correspond to quasi-elastic process whereas bins II, III & IV possibly represent deep-inelastic or quasi fission processes.

Fig. 13: The average values and standard deviations of scattering angles and asymmetries ($\zeta = (A_1-A_2)/(A_1+A_2)$) corresponding to the three TKEL bins in the reaction $^{84}Kr + ^{238}U$ at 12.5 MeV/u. For the $150 \leq$ TKEL ≤ 450 bin two distinct scattering angle and asymmetry groups can be identified. Group II corresponds to deep-inelastic process and group III is most probably a quasi-fission-like reaction mechanism. Group I is unambignously quasi-elastic reactions, whereas group IV having a broad asymmetry distribution, large scattering angle and very high kinetic-energy loss is probably a combination of deep-inelastic and quasi-fission processes. The entrance channel asymmetry ($\zeta = 0.48$) and the quarter-point angle ($\xi_{\frac{1}{4}} = 24.9^{\circ}$) is also indicated on the diagram.

Fig. 14: The projected lengths of the three four-pronged events and the angles between them, for the reaction $^{84}Kr + ^{238}U$ at 12.5 MeV/u Event no III is clearly a four-pronged event, however, because of a very small (and broad) projected view of one of the tracks it could not be analyzed numerically.

Fig. 15: The distribution of relative velocities $v_{23} = |\vec{v}_2 - \vec{v}_3|$ and $v_{14} = |\vec{v}_1 - \vec{v}_4|$ of the complementary pairs of final masses produced in the reaction $^{84}Kr + ^{238}U$ at 12.5 MeV/u. The standard deviations of the gaussian fits $\sigma_{v_{14}}$ and $\sigma_{v_{23}}$ correspond to the experimental errors alone. Arrows indicate mean values of empirical relative velocities in the case of pairs arising from sequential fission.

Fig. 16: The distributions of final masses for the two direct quarternary events observed in the reaction $^{84}Kr + ^{238}U$ at 12.5 MeV/u. The standard deviations of gaussian fits represent the experimental errors alone. One pair of masses in each event arises from sequential fission. The corresponding prefission masses for these pairs are also indicated.

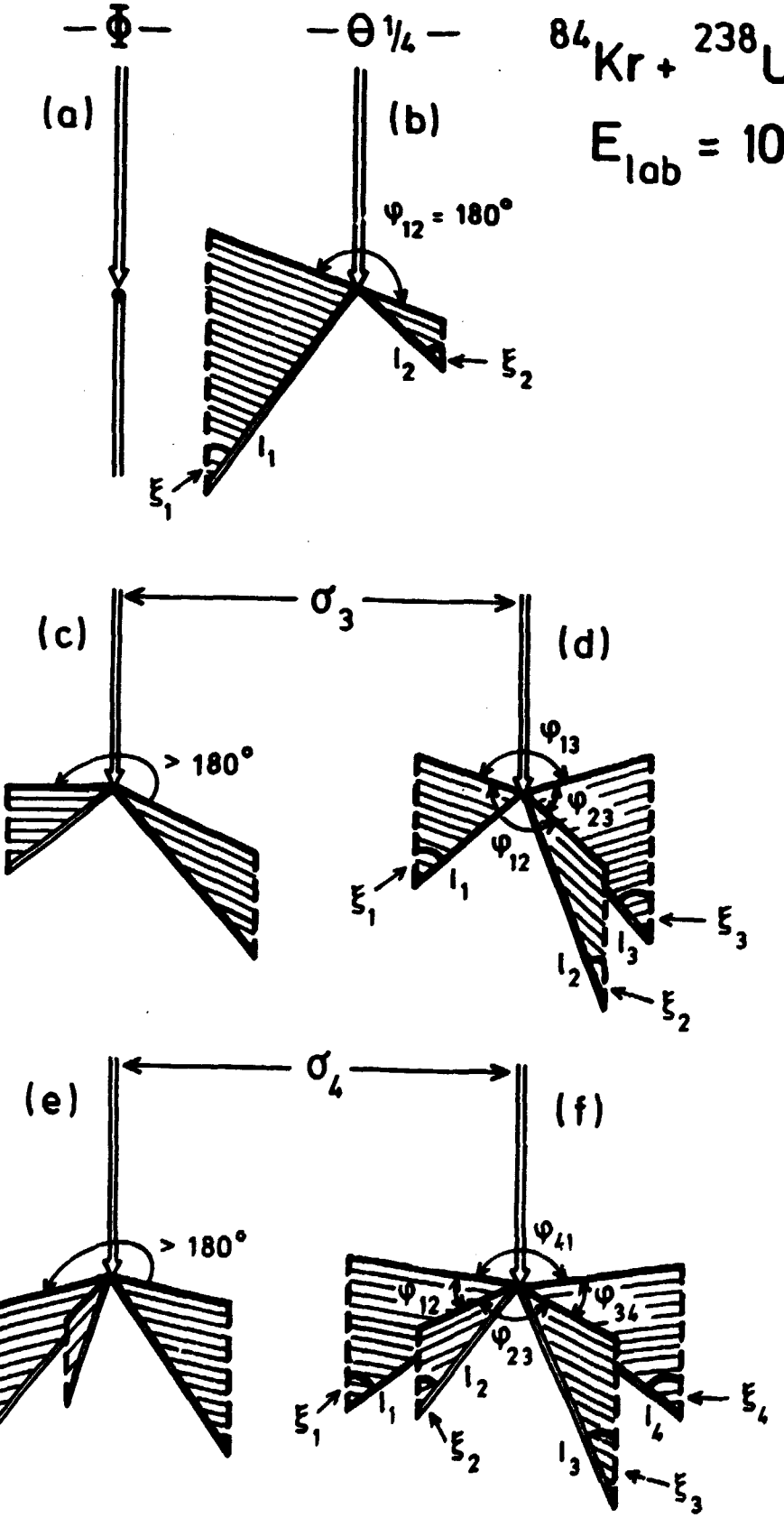
−Φ−
−Θ¼−
(a)
(b)
$^{84}Kr + ^{238}U$
E_{lab} = 1050 MeV
$\varphi_{12} = 180°$
l_2
ξ_2
l_1
ξ_1
σ_3
(c)
(d)
> 180°
φ_{13}
φ_{23}
φ_{12}
ξ_1
l_1
ξ_3
l_3
l_2
ξ_2
σ_4
(e)
(f)
> 180°
φ_{41}
φ_{12}
φ_{34}
φ_{23}
l_2
ξ_1
l_1
ξ_2
ξ_4
l_4
l_3
ξ_3

Fig. 1

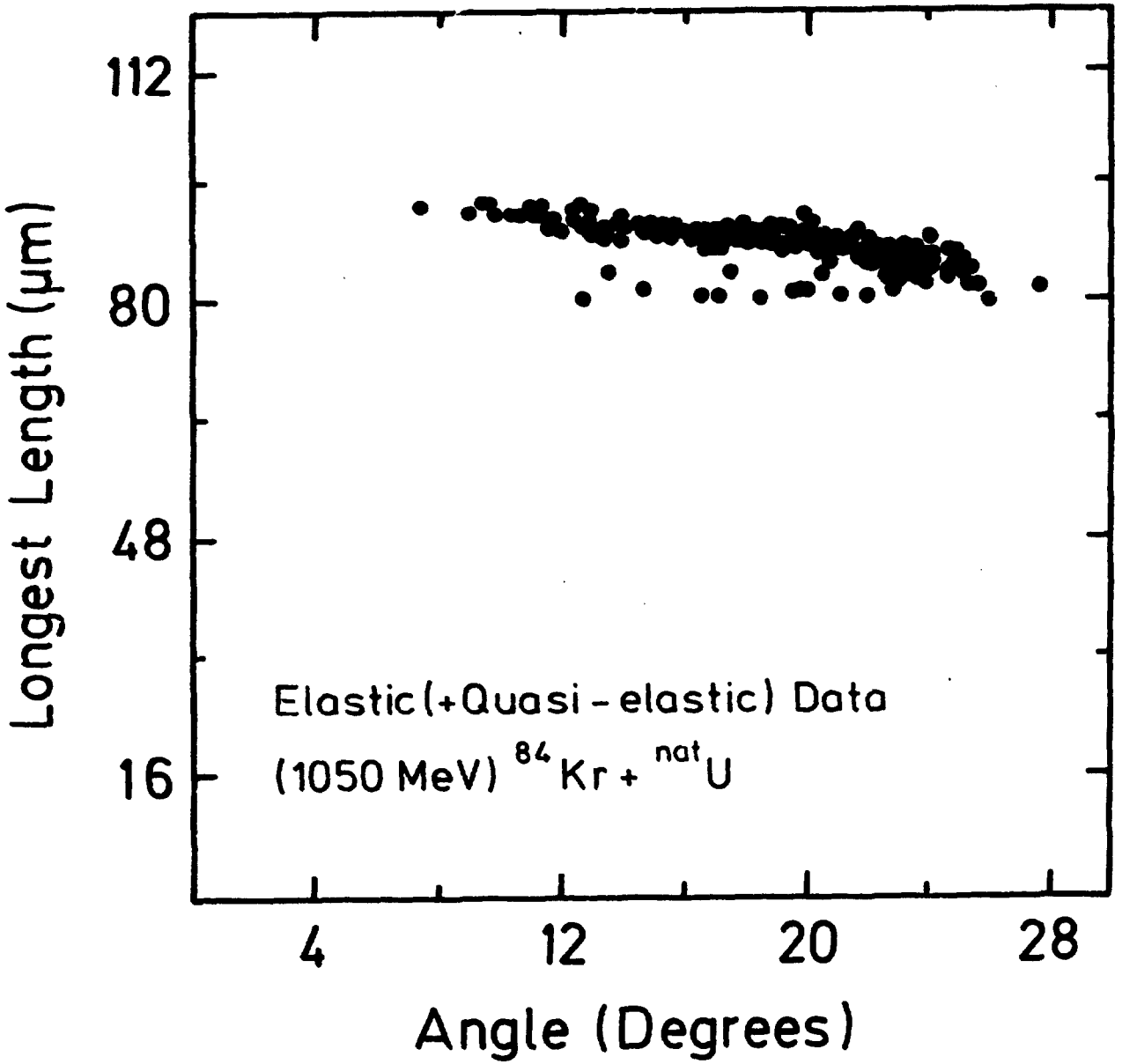
112
80
48
16
Longest Length (μm)
Elastic (+Quasi - elastic) Data
(1050 MeV) ^{84}Kr + ^{nat}U
4
12
20
28
Angle (Degrees)

Fig. 2

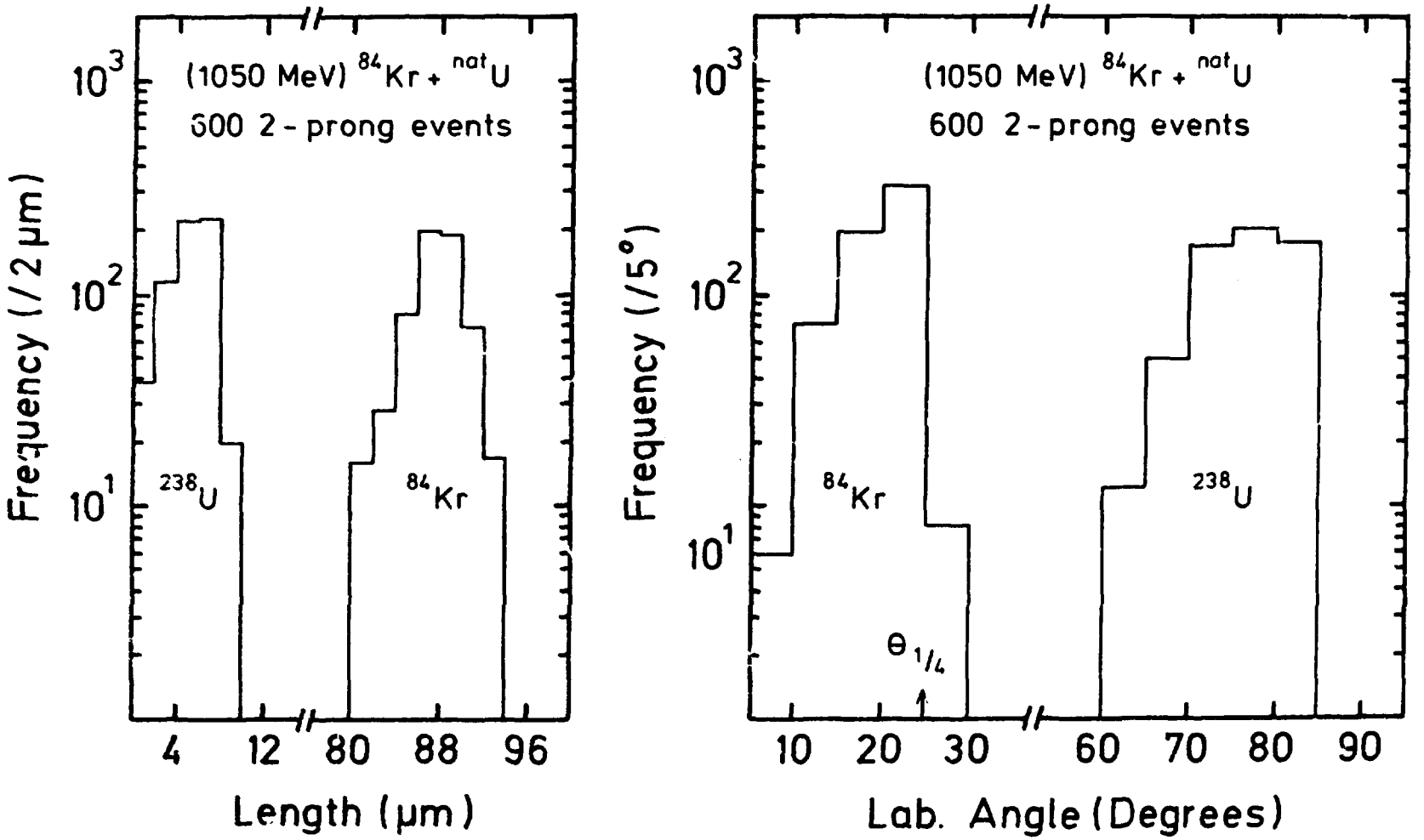
(1050 MeV) ^{84}Kr + ^{nat}U
600 2-prong events
Frequency (/2 μm)
10^3
10^2
10^1
^{238}U
^{84}Kr
4
12
80
88
96
Length (μm)
(1050 MeV) ^{84}Kr + ^{nat}U
600 2-prong events
Frequency (/5°)
^{84}Kr
^{238}U
$\theta_{1/4}$
10
20
30
60
70
80
90
Lab. Angle (Degrees)

Fig. 3

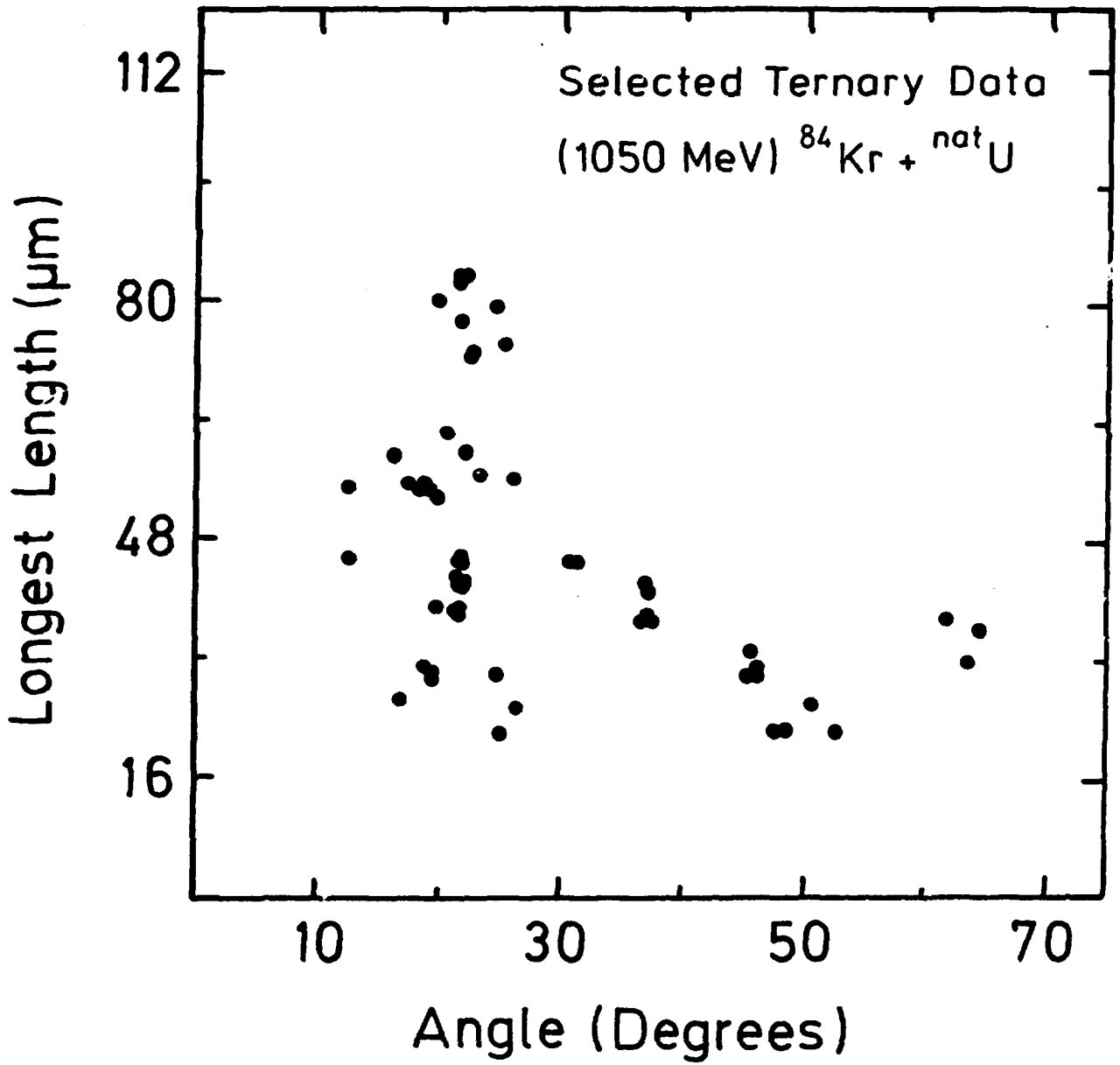
Selected Ternary Data
(1050 MeV) $^{84}Kr + ^{nat}U$
Longest Length (μm)
112
80
48
16
10
30
50
70
Angle (Degrees)

Fig. 4

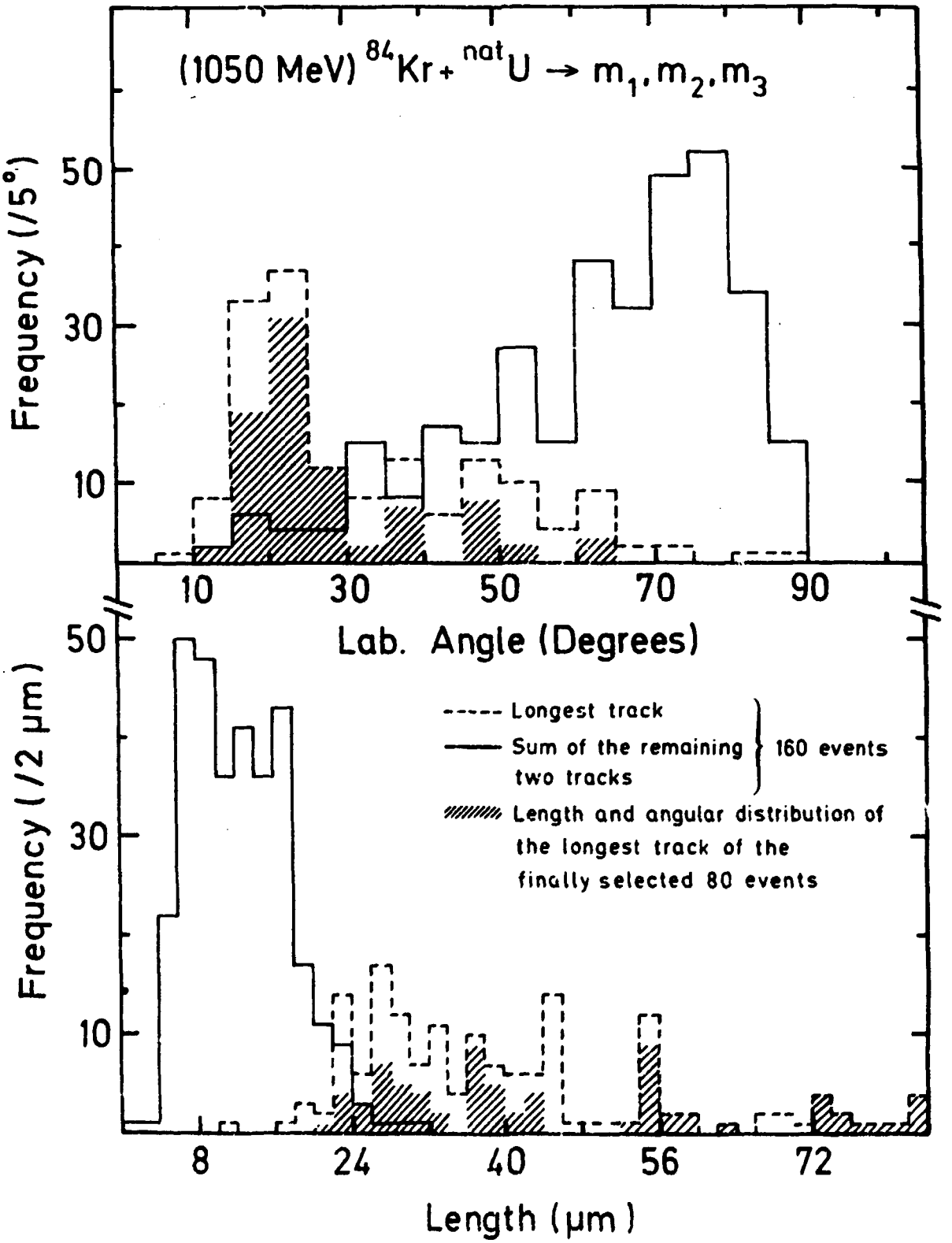
(1050 MeV) $^{84}Kr + ^{nat}U \rightarrow m_1, m_2, m_3$
Frequency (/5°)
50
30
10
10
30
50
70
90
Lab. Angle (Degrees)
Frequency (/2 μm)
50
30
10
----- Longest track
—— Sum of the remaining two tracks
160 events
Length and angular distribution of the longest track of the finally selected 80 events
8
24
40
56
72
Length (μm)

Fig. 5

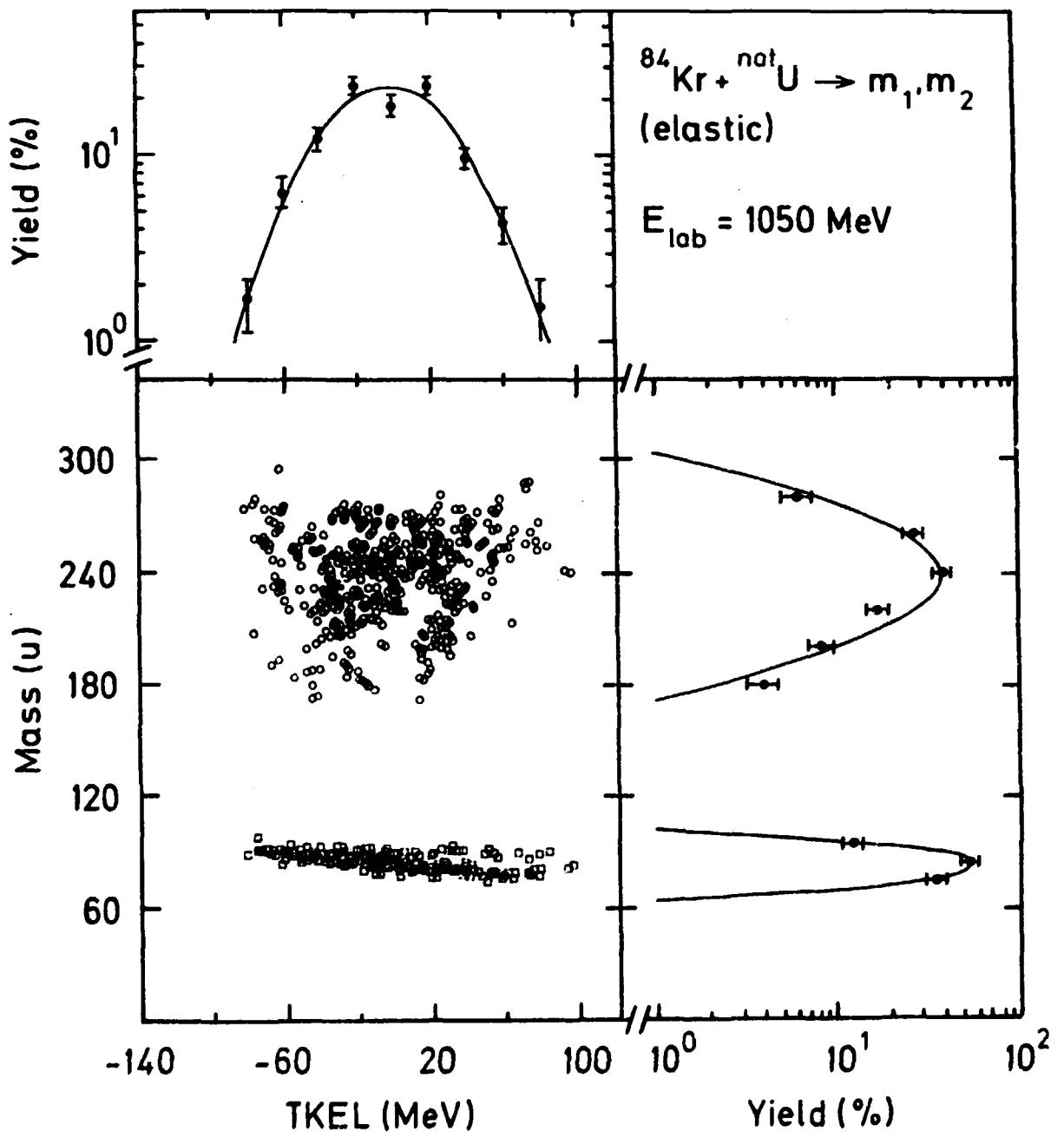
Yield (%)
10^1
10^0
$^{84}Kr + ^{nat}U \rightarrow m_1, m_2$
(elastic)
E_{lab} = 1050 MeV
Mass (u)
300
240
180
120
60
-140
-60
20
100
TKEL (MeV)
10^0
10^1
10^2
Yield (%)

Fig. 6

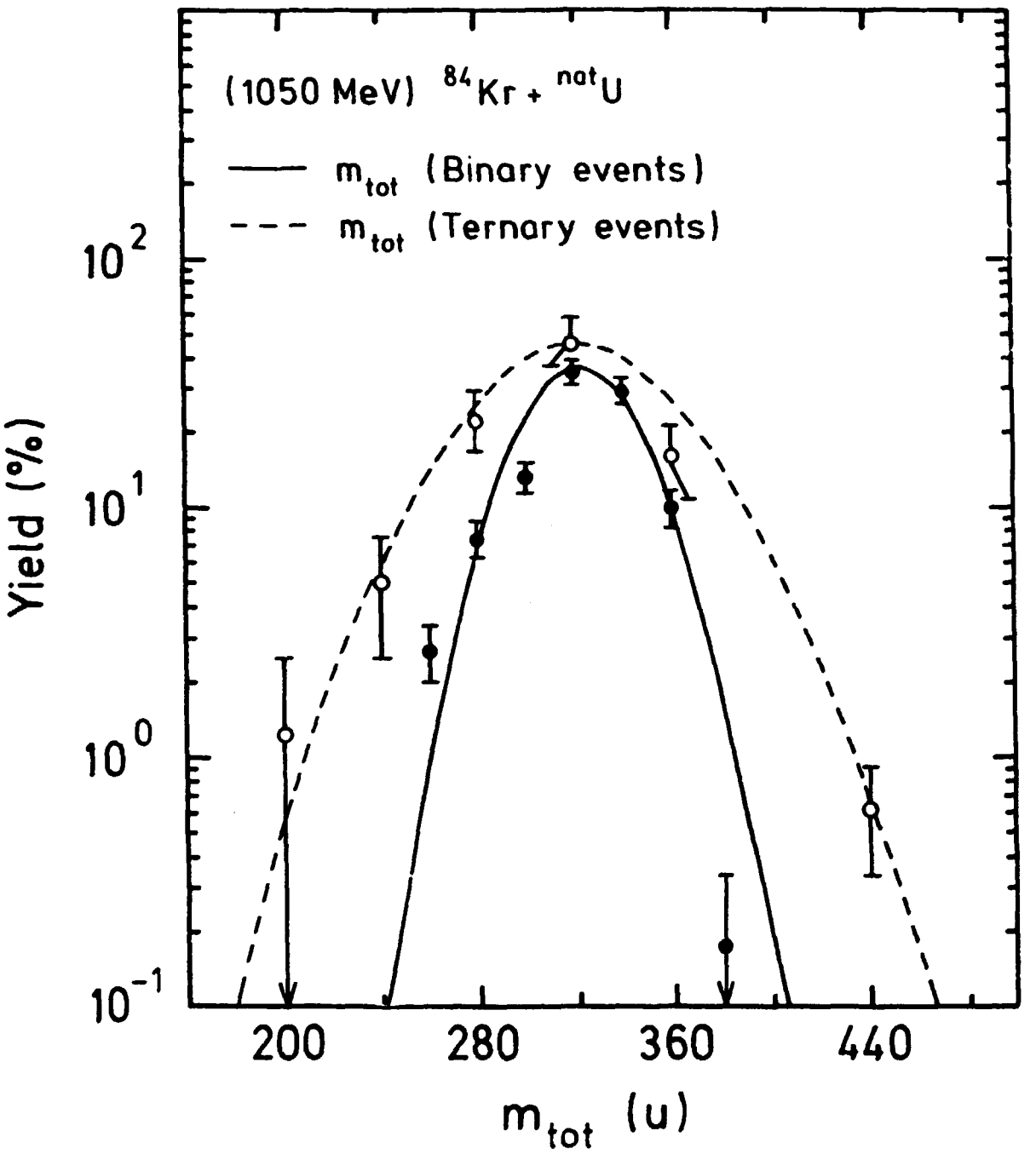
(1050 MeV) $^{84}Kr + ^{nat}U$
m_{tot} (Binary events)
m_{tot} (Ternary events)
Yield (%)
10^2
10^1
10^0
10^{-1}
200
280
360
440
m_{tot} (u)

Fig. 7

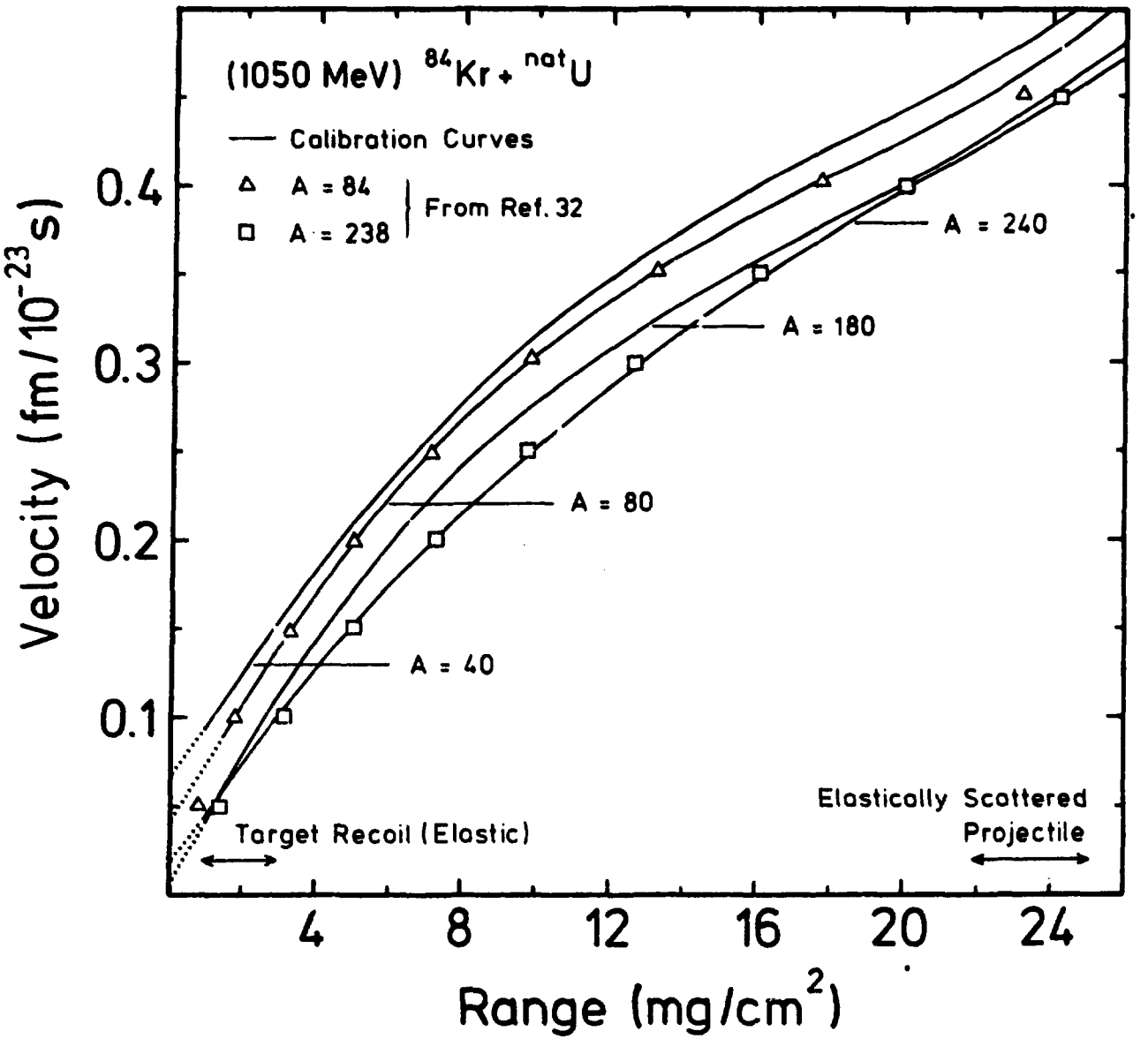
(1050 MeV) $^{84}Kr + ^{nat}U$
Calibration Curves
A = 84
A = 238
From Ref. 32
A = 240
A = 180
A = 80
A = 40
Target Recoil (Elastic)
Elastically Scattered Projectile
Velocity (fm/10^{-23}s)
Range (mg/cm^2)
0.1
0.2
0.3
0.4
4
8
12
16
20
24

Fig. 8

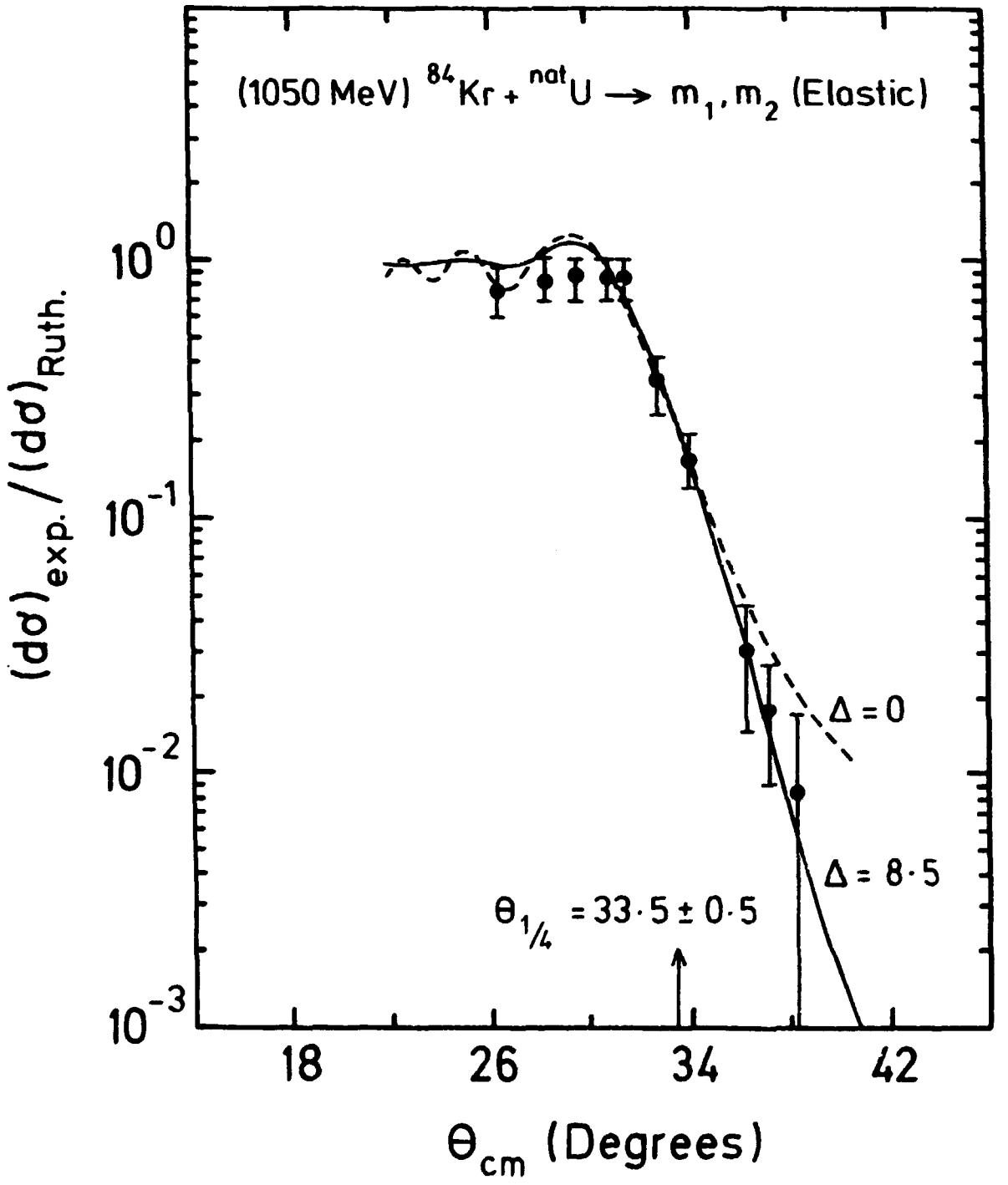
(1050 MeV) $^{84}Kr + ^{nat}U \rightarrow m_1, m_2$ (Elastic)
$(d\sigma)_{exp.} / (d\sigma)_{Ruth.}$
10^0
10^{-1}
10^{-2}
10^{-3}
$\Delta = 0$
$\Delta = 8{\cdot}5$
$\theta_{1/4} = 33{\cdot}5 \pm 0{\cdot}5$
18
26
34
42
θ_{cm} (Degrees)

Fig. 9

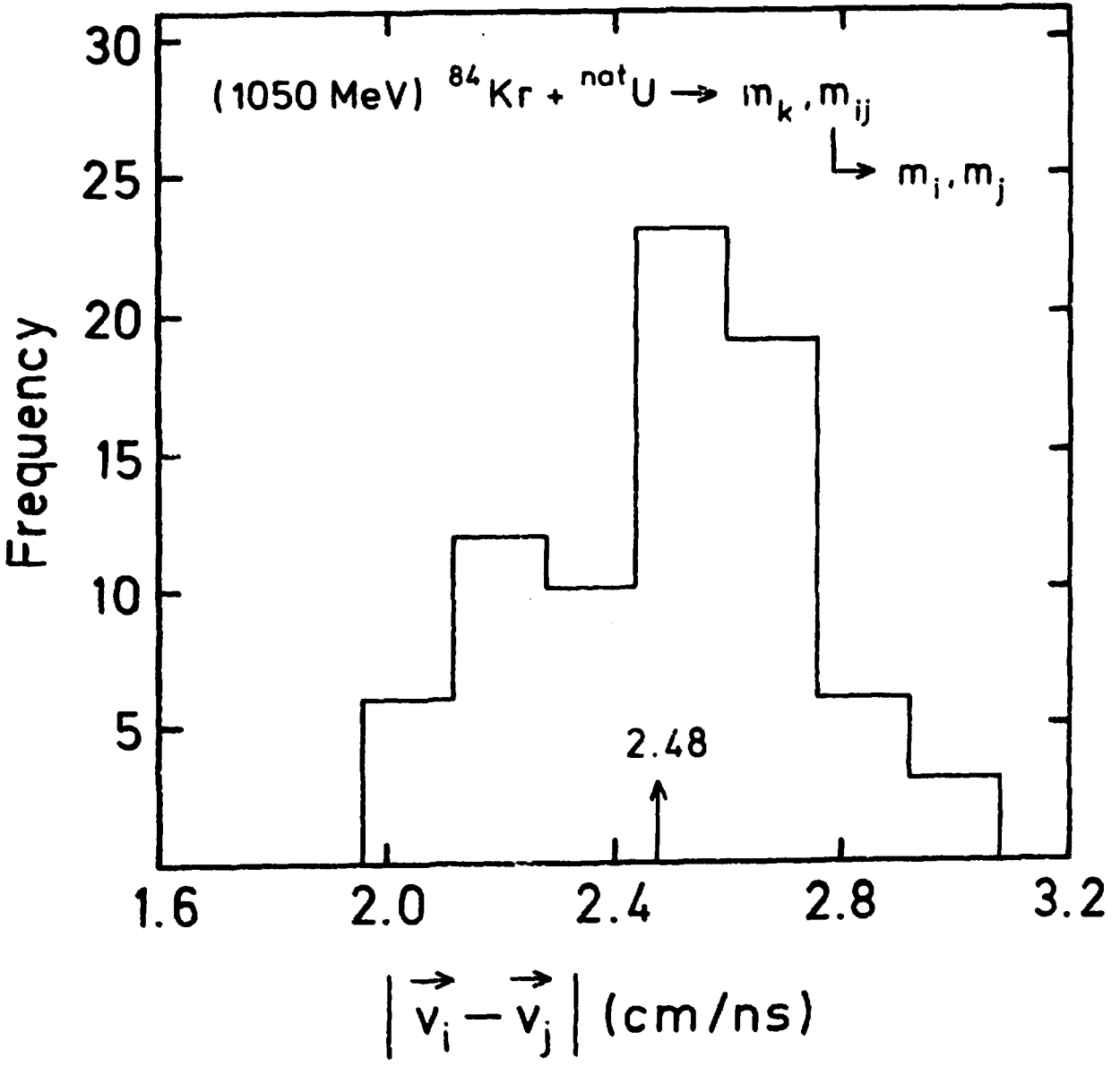
(1050 MeV) $^{84}Kr + ^{nat}U \rightarrow m_k, m_{ij}$
$\hookrightarrow m_i, m_j$
Frequency
30
25
20
15
10
5
2.48
1.6
2.0
2.4
2.8
3.2
$|\vec{v}_i - \vec{v}_j|$ (cm/ns)

Fig. 10

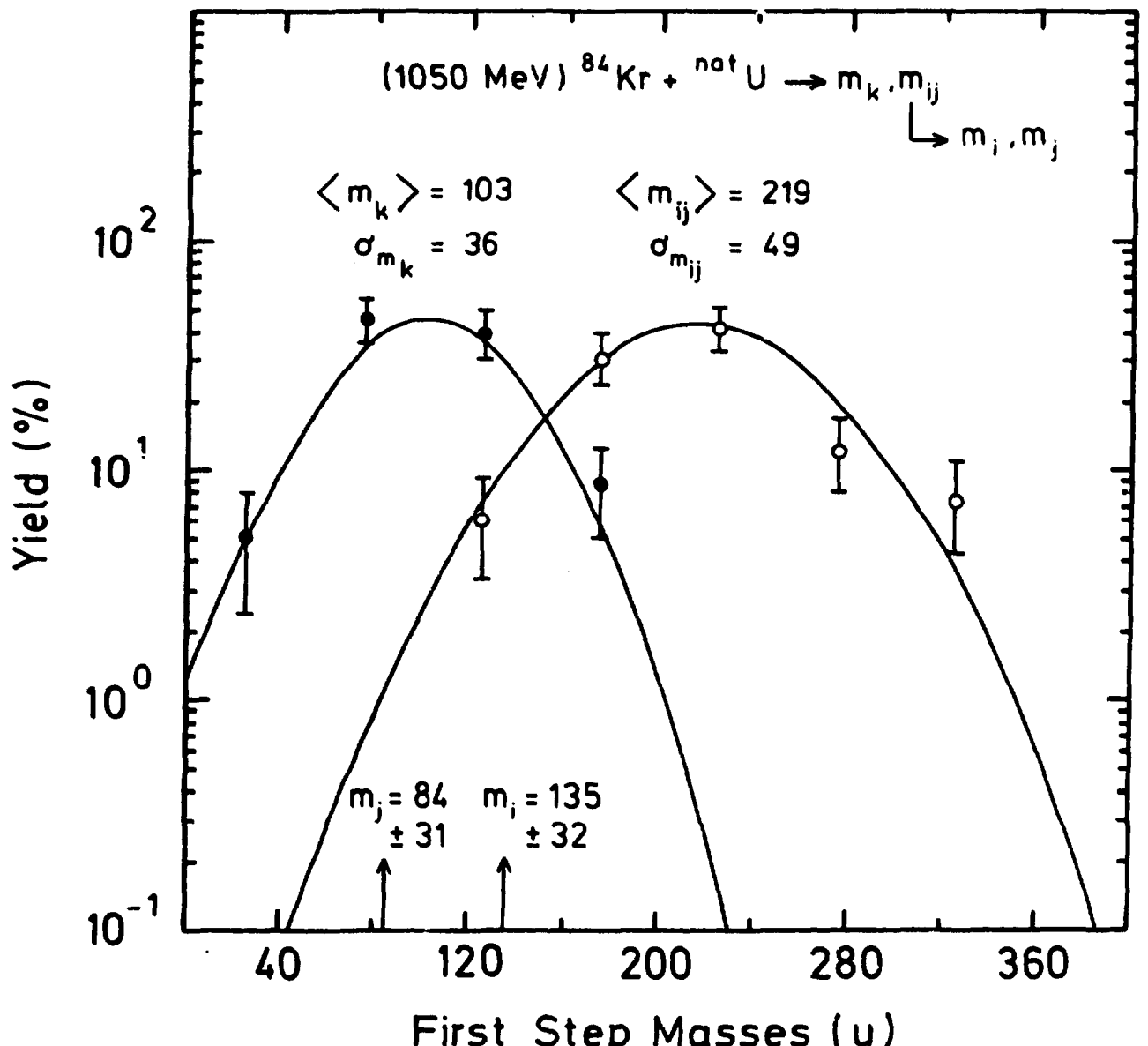
(1050 MeV) $^{84}Kr + ^{nat}U \rightarrow m_k, m_{ij}$
$\hookrightarrow m_i, m_j$
$\langle m_k \rangle = 103$
$\sigma_{m_k} = 36$
$\langle m_{ij} \rangle = 219$
$\sigma_{m_{ij}} = 49$
$m_j = 84 \pm 31$
$m_i = 135 \pm 32$
Yield (%)
10^2
10^1
10^0
10^{-1}
40
120
200
280
360
First Step Masses (u)

Fig. 11

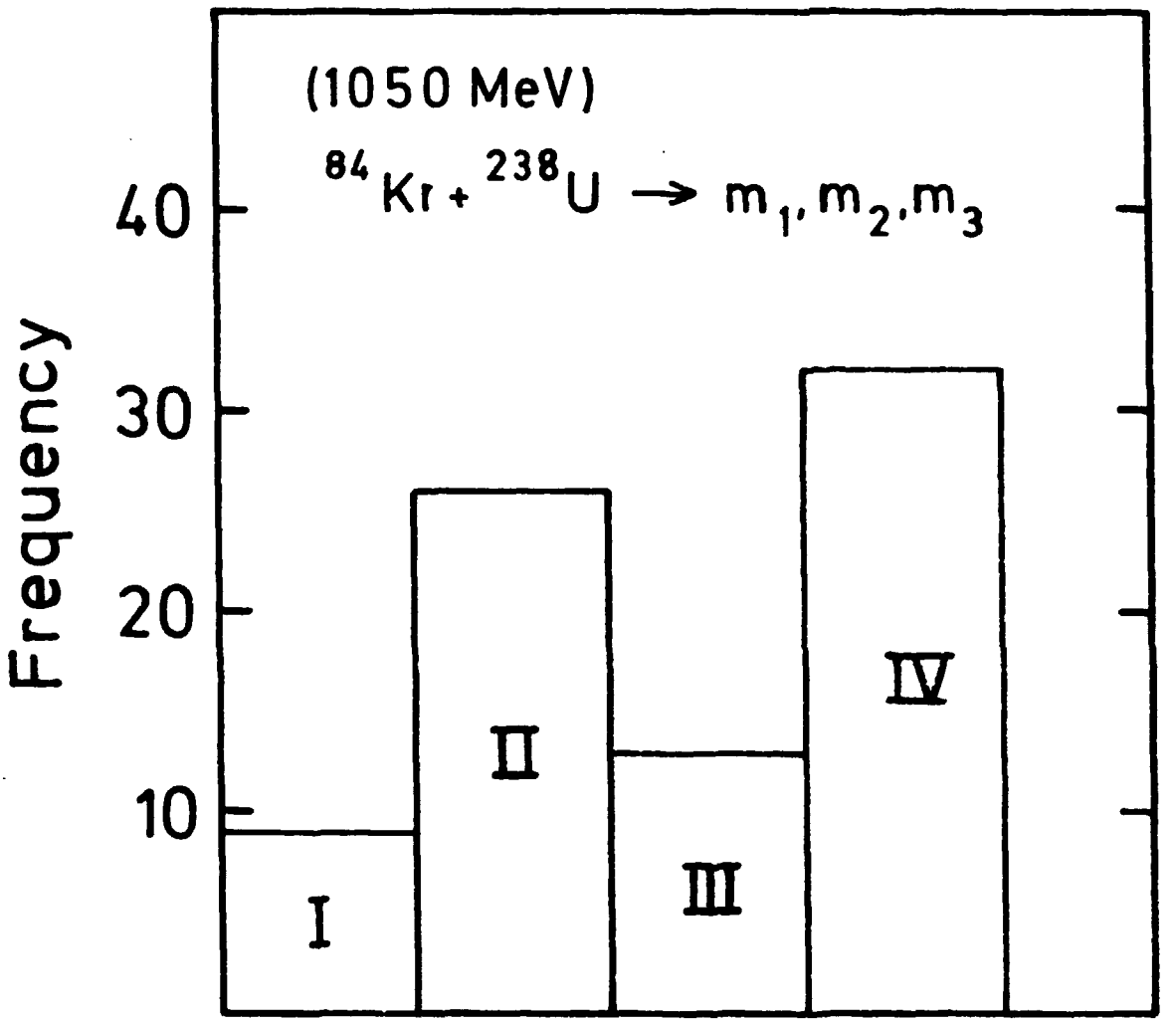

I: $-150 < TKEL < 150$; $\bar{\xi} = 23 \pm 2$

II: $150 < TKEL < 450$; $\bar{\xi} = 21 \pm 3$

III: $150 < TKEL < 450$; $\bar{\xi} = 65 \pm 9$

IV: $TKEL > 450$; $\bar{\xi} = 60 \pm 17$

Fig. 12

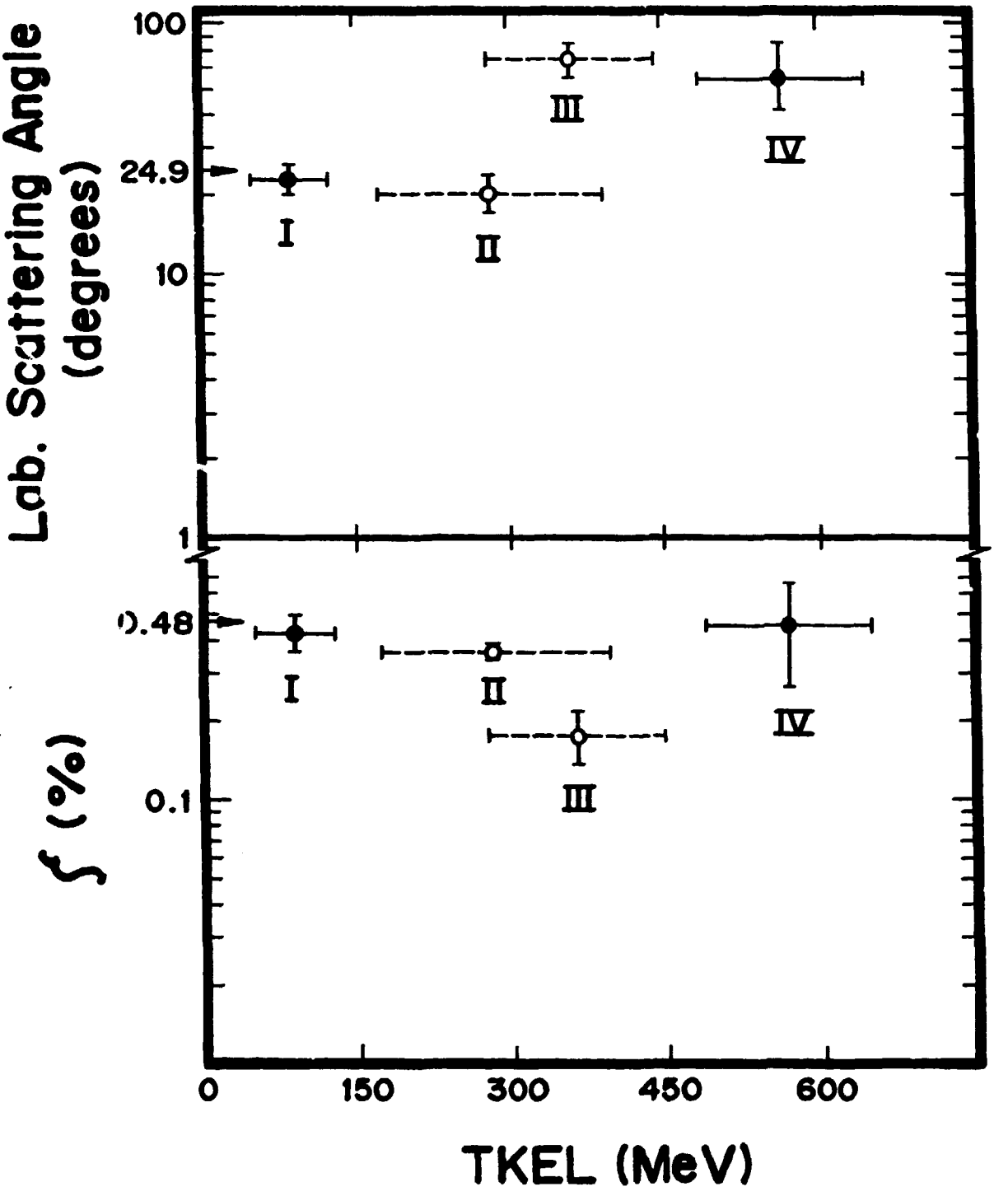
Lab. Scattering Angle (degrees)
100
24.9
10
1
0.48
0.1
I
II
III
IV
f (%)
0
150
300
450
600
TKEL (MeV)

Fig. 13

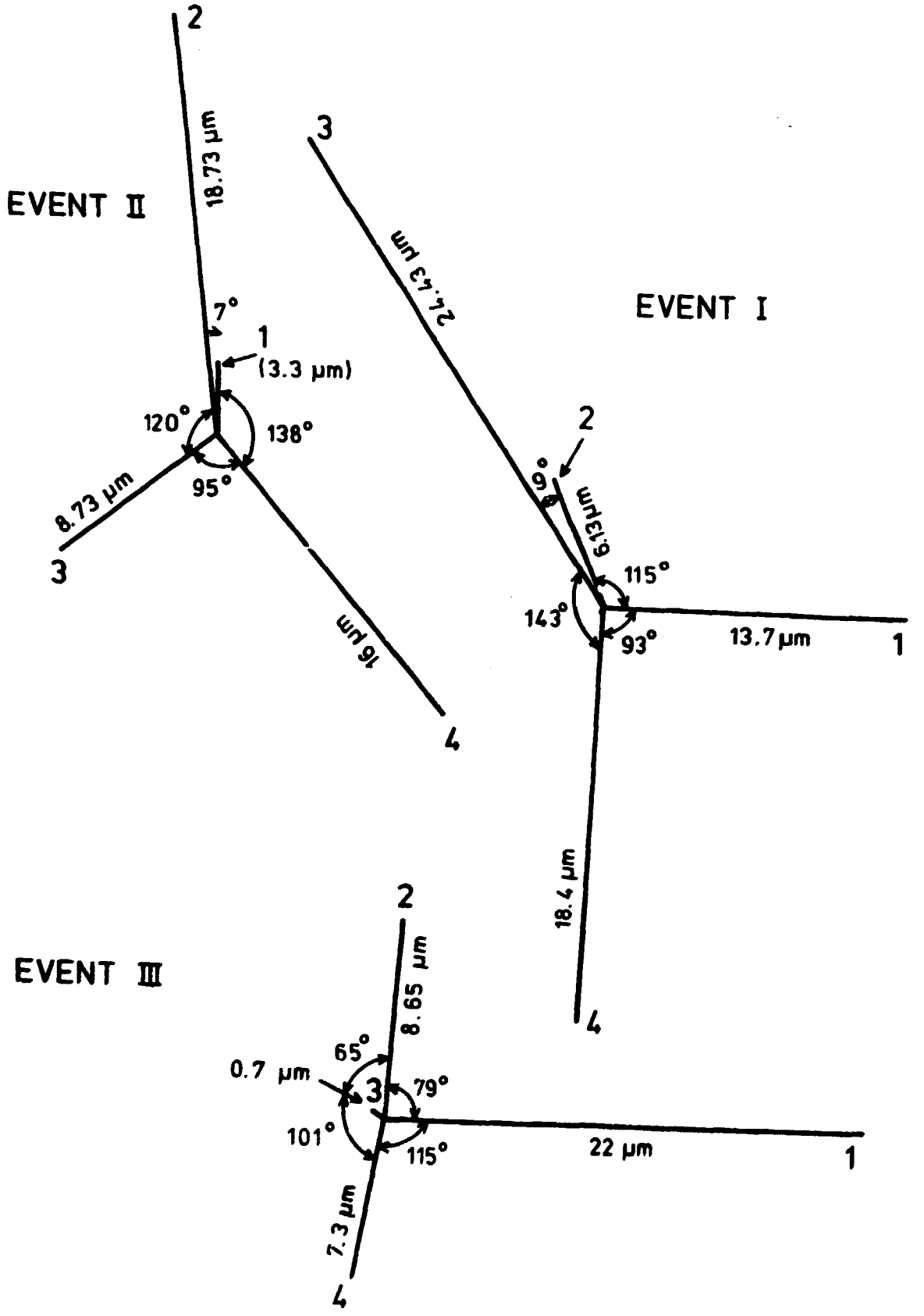
EVENT II
2
18.73 µm
7°
1
(3.3 µm)
120°
138°
95°
8.73 µm
3
16 µm
4
EVENT I
3
24.43 µm
2
9°
6.13µm
115°
143°
93°
13.7 µm
1
18.4 µm
4
EVENT III
2
8.65 µm
65°
0.7 µm
3
79°
101°
115°
22 µm
1
7.3 µm
4

Fig. 14

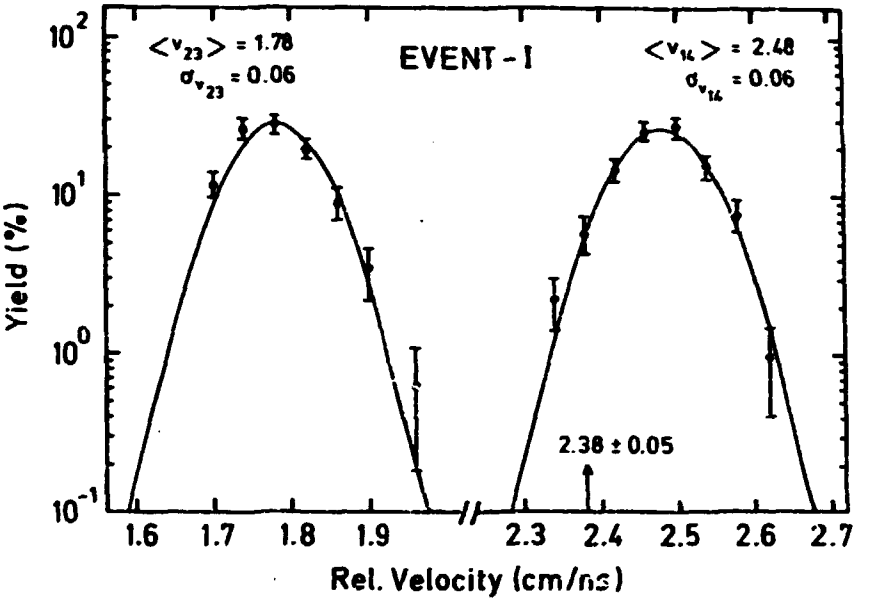
EVENT - I
$\langle v_{23} \rangle$ = 1.78
$\sigma_{v_{23}}$ = 0.06
$\langle v_{14} \rangle$ = 2.48
$\sigma_{v_{14}}$ = 0.06
2.38 ± 0.05
Yield (%)
Rel. Velocity (cm/ns)

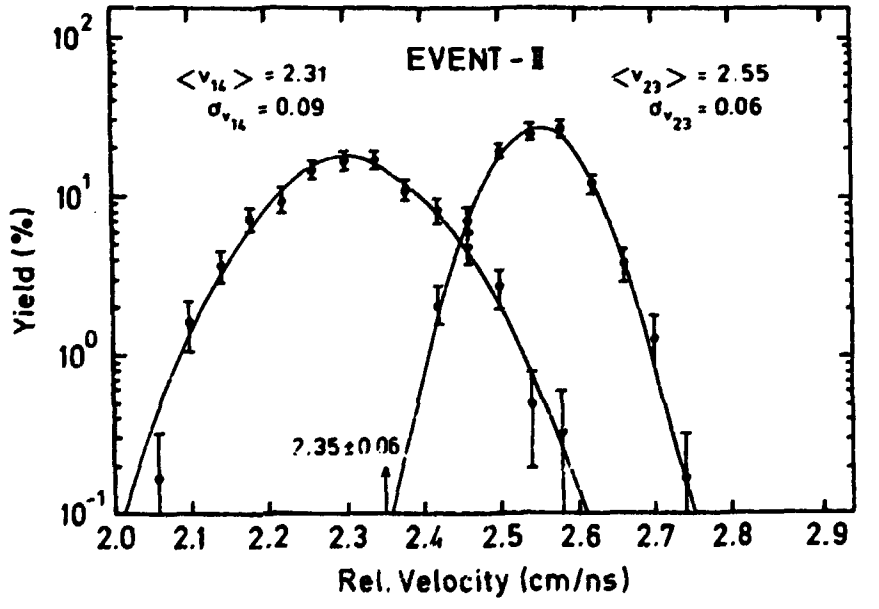
EVENT - II
$\langle v_{14} \rangle$ = 2.31
$\sigma_{v_{14}}$ = 0.09
$\langle v_{23} \rangle$ = 2.55
$\sigma_{v_{23}}$ = 0.06
2.35 ± 0.06
Yield (%)
Rel. Velocity (cm/ns)

Fig. 15

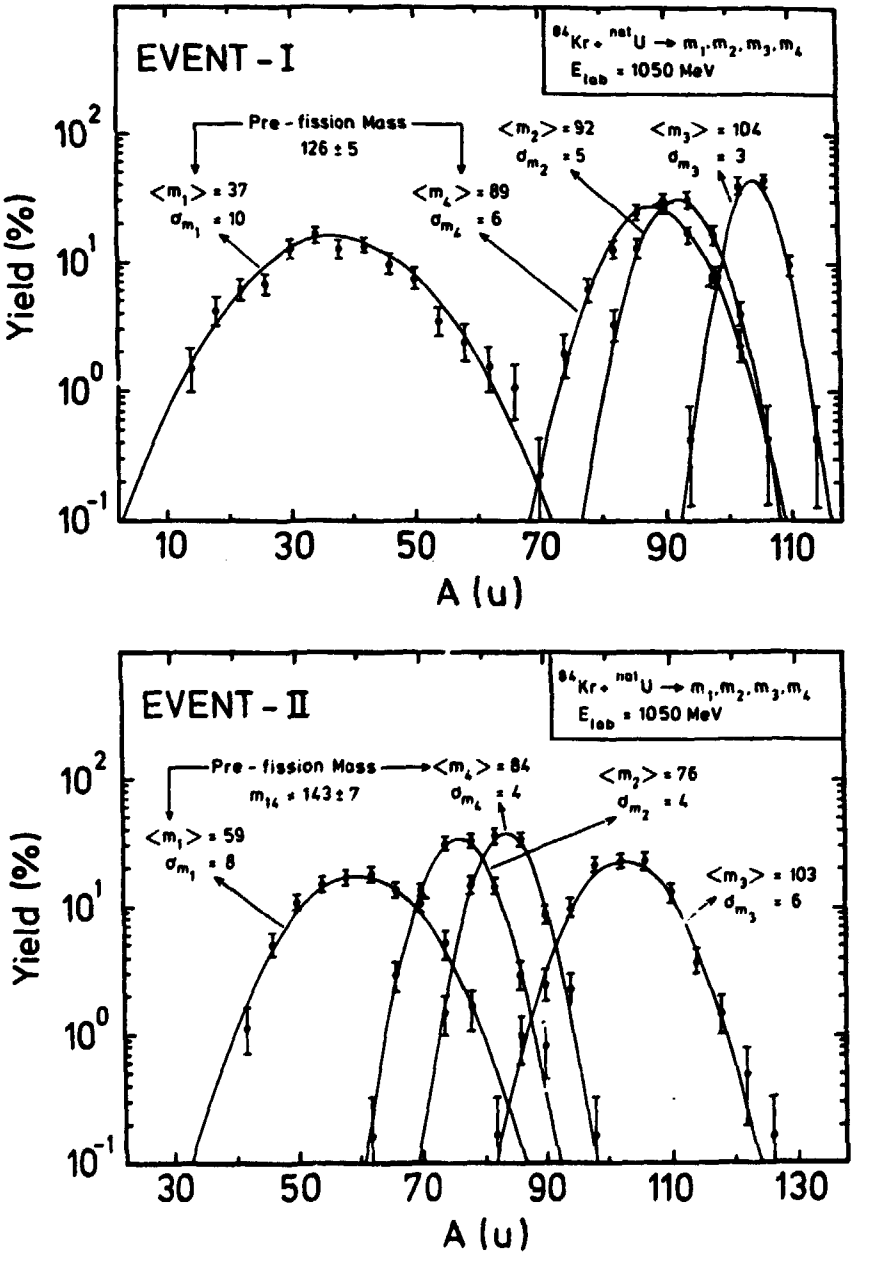
EVENT - I
$^{84}Kr + ^{nat}U \rightarrow m_1, m_2, m_3, m_4$
E_{lab} = 1050 MeV
Pre - fission Mass
126 ± 5
$\langle m_1 \rangle$ = 37
σ_{m_1} = 10
$\langle m_4 \rangle$ = 89
σ_{m_4} = 6
$\langle m_2 \rangle$ = 92
σ_{m_2} = 5
$\langle m_3 \rangle$ = 104
σ_{m_3} = 3
Yield (%)
A (u)
EVENT - II
$^{84}Kr + ^{nat}U \rightarrow m_1, m_2, m_3, m_4$
E_{lab} = 1050 MeV
Pre - fission Mass
m_{14} = 143 ± 7
$\langle m_4 \rangle$ = 84
σ_{m_4} = 4
$\langle m_2 \rangle$ = 76
σ_{m_2} = 4
$\langle m_1 \rangle$ = 59
σ_{m_1} = 8
$\langle m_3 \rangle$ = 103
σ_{m_3} = 6
Yield (%)
A (u)

Fig. 16